1   **TITLE:** Specimen alignment with limited point-based homology: 3D morphometrics of
2   disparate bivalve shells (Mollusca: Bivalvia)

3   **RUNNING HEAD:** Aligning bivalve shells

4   **KEYWORDS:** marine bivalve, shell shape, geometric morphometrics, 3D morphometrics,
5   anatomical homology

6   **AUTHORS:** Stewart M. Edie[1*], Katie S. Collins[2], David Jablonski[3,4]

7   [1] Department of Paleobiology, National Museum of Natural History, Smithsonian Institution,
8   Washington, DC, 20013, U.S.A.

9   [2] Natural History Museum, London, London, SW7 5BD, United Kingdom

10   [3] Department of the Geophysical Sciences, University of Chicago, 5734 South Ellis Ave,
11   Chicago, IL 60637, USA.

12   [4] Committee on Evolutionary Biology, University of Chicago, Chicago, IL 60637, USA

13   * corresponding author

14

15   1.   Abstract

16   Comparative morphology fundamentally relies on the orientation and alignment of specimens. In
17   the era of geometric morphometrics, point-based homologies are commonly deployed to register
18   specimens and their landmarks in a shared coordinate system. However, the number of point-
19   based homologies commonly diminishes with increasing phylogenetic breadth. These situations
20   invite alternative, often conflicting, approaches to alignment. The bivalve shell (Mollusca:
21   Bivalvia) exemplifies a homologous structure with few universally homologous points—only
22   one can be identified across the Class, the shell 'beak.' Here, we develop an axis-based
23   framework, grounded in the homology of shell features, to orient shells for landmark-based,
24   comparative morphology. As the choice of homologous points for alignment can affect shape
25   differences among specimens, so can the choice of orientation axes. Analysis of forty-five
26   possible alignment schemes finds general conformity among the shape differences of 'typical'
27   equilateral shells, but the shape differences among atypical shells can change considerably,
28   particularly those with distinctive modes of growth. Each alignment implies a hypothesis about
29   the ecological, developmental, or evolutionary basis of morphological differences, but we
30   recognize one alignment in particular as a continuation of the historical approaches to
31   morphometrics of shell form: orientation via the hinge line. Beyond bivalves, this axis-based

32   approach to aligning specimens facilitates the comparison of continuous differences in shape
33   among many other phylogenetically broad and morphologically disparate samples.

2.   Introduction

35   Comparative morphology depends on how organisms are oriented, or aligned. For a simplistic
36   example, a kiwi's beak is relatively long for a bird when measured from the tip to the base of the
37   skull, but rather short when measured from the tip to the nostrils (an alternative definition of
38   beak length; Borras et al. 2000). Thus, the choice of anatomical reference points can profoundly
39   alter our interpretations of evolutionary morphology. Alignments commonly use point-based
40   aspects of homologous features—the junction of the kiwi's beak with the cranium (a Type I
41   landmark; Bookstein 1992) and the distal-most point of the beak, the tip (a Type III landmark).
42   Closely related organisms tend to have more of these homologous points, allowing for a
43   straightforward alignment and comparison of their shapes. Alignment on strict, point-based
44   homology becomes more problematic with increasing phylogenetic distance, however, as the
45   number of homologous features invariably diminishes (Bardua et al. 2019).

46   Bivalve mollusks have become a model system for macroevolution and macroecology
47   (Jablonski et al. 2017; Edie et al. 2018; Crame 2020), but their strikingly disparate body plans
48   complicate Class-wide morphologic comparisons using strict homology (Cox et al. 1969).
49   Inimical to triangulation and thus alignment via landmarks, the valve of the bivalve shell—the
50   most widely available feature of the animal today and through the fossil record—has only one
51   homologous *point*: the apex of the beak, which is the origin of growth of the embryonic shell at
52   the apex of the beak (Carter et al. 2012:21; Figure 1). Homology-free approaches can be useful
53   for comparing the shapes of shell valves when anatomical orientation is either unknown or
54   uncertain (Bailey 2009); but wholesale substitution of shape, i.e. analogy, for homology
55   complicates the evolutionary interpretation of morphological differences. Despite the lack of
56   multiple homologous *points* on the shell valve across the Class, a number of its *features* are
57   homologous and can facilitate comparisons. Here, we apply principles of bivalve comparative
58   morphology to develop a framework for aligning shell valves (hereafter 'shells') across the Class,
59   thus enabling phylogenetically extensive analyses of their shapes using geometric morphometrics
60   despite the remarkable range of body plans across the clade.

2.1   Approaches to orienting the bivalve shell

62   Many body directions, axes, lines, and planes have been defined for bivalves (see Cox et al.
63   1969; Bailey 2009; Carter et al. 2012)—some related to features of the shell (an accretionary
64   exoskeleton composed of calcium carbonate; Marin et al. 2012), and others to features of the soft
65   body (the digestive tract, foot, byssus, muscles, etc.). Separation into these 'shell' and 'body'

66   terms is a false (Stasek 1963*a*) but convenient dichotomy (Yonge 1954): the shell is generated

67   by, and remains attached to, the soft body, but their morphologies can become decoupled (Yonge

68   1954; Edie et al. 2022). Still, both shell and body features are required for orientation via

69   homology (Stasek 1963*a*; cf. Bailey 2009). Given our goal of aligning the shell for geometric

70   morphometrics across broad phylogenetic scales and through the fossil record, we focus on

71   orientations that can be inferred from this part alone, but we must use a critical body axis to fully

72   determine orientation, the anteroposterior axis. Thus, shell features used for alignment can be

73   divided into two classes: (1) intrinsic characteristics of the shell relating to its geometry, growth,

74   and biomechanics, and (2) proxies of the body recording the positions of the soft anatomy

75   including the adductor muscle scars, pallial line, byssal notch, pedal gape, siphon canal, and

76   more.

2.1.1   Orientation via intrinsic characteristics of the shell

78   Although the only homologous point on the shell across all bivalves is the apex of the beak

79   (hereafter 'beak', Figure 1), aspects of the shell's biomechanics, such as its hinge axis, and its

80   accretionary growth permit orientation via homology. The planes and lines proposed to describe

81   shell geometry and growth have been criticized for their lack of homology (Stasek 1963b:226)

82   and ubiquity across the class (Lison 1949:62; Owen 1952:149; Carter 1967:272). We discuss two

83   such features here, the directive plane and demarcation line (Figure 1 and defined below), but we

84   also address and test two alternative means of orienting shells that combine the shell's geometry

85   and growth: the maximum growth axis and the shape of the shell commissure.

86   Related to the shell's biomechanics, the hinge has been treated as a "fixed dorsal region"

87   (Yonge 1954:448; see also Jackson 1890:282), later redefined to reflect the position of the

88   mantle isthmus bridging between the two valves as a universally dorsal-directed feature (Cox et

89   al. 1969:79). Beyond its determination of dorsoventral directionality, the hinge, specifically the

90   hinge axis defined as the "ideal line drawn through the hinge area, and coinciding with the axis

91   of motion of the valves" (Jackson 1890:309), is a Class-wide feature that can constrain one of the

92   three Cartesian axes required for alignment. In a strictly mechanical sense, the ligament, and not

93   the hinge teeth, directs the orientation of the axis of motion (Trueman 1964:56; Cox et al.

94   1969:47; Stanley 1970:47). However, the hinge area, which includes the teeth, is hypothesized to

95   be analogous in function (Cox et al. 1969:47)—guiding the two valves into alignment during

96   closure—and homologous in its origin (Scarlato and Starobogatov 1978; Waller 1998; Fang and

97   Sanchez 2012). Thus, our definition of the **hinge line** indicates the longest dimension of the

98   hinge area (see 'hinge' in Carter et al. 2012:74 and Figure 1); for quantitatively aligning shells,

99   the hinge line is determined by the two farthest apart articulating elements of the hinge area,

100   excluding lateral teeth, which are variably present among heterodont species (e.g. Mikkelsen et

101 al. 2006:493; Taylor and Glover 2021); definition proposed here is a synthesis of the discussions

102 in Cox et al. 1969:81 and Bradshaw and Bradshaw 1971). Thus, by directing the orientation of

103 the horizontal plane which divides the body into dorsal (towards the beak) and ventral (towards

104 the free edge of the shell) territories, the hinge line can also proxy the anteroposterior axis

105 (Figure 1, Cox et al. 1969:81 and discussion below).

106
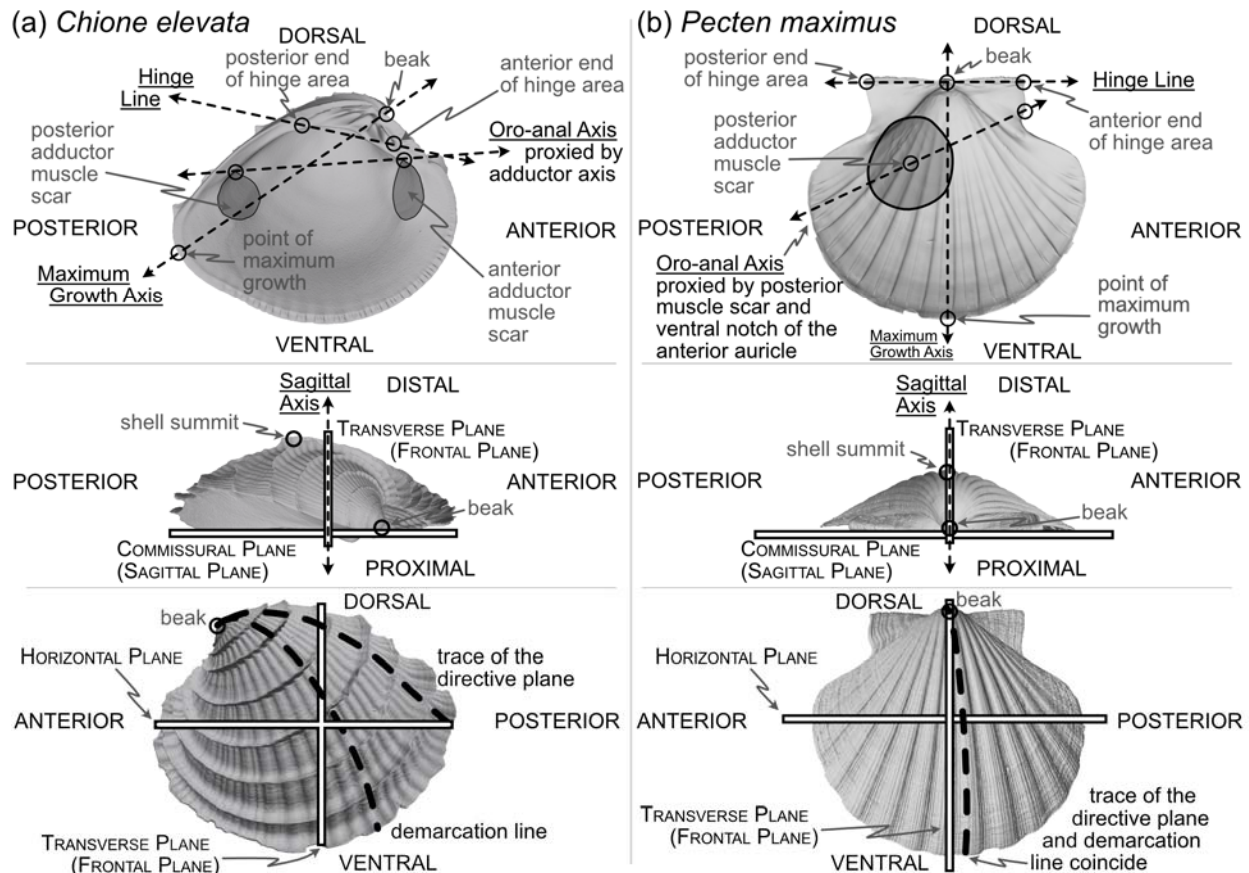
Figure 1. Positions of shell features, axes, and planes as mentioned and defined in text for: (a) a helicospiral shell *Chione elevata* (Say 1822), and (b) a more planispiral shell *Pecten maximus* (Linnaeus 1767).

111 Related to the geometry and growth of the shell, the **directive plane** (Lison 1949) was

112 proposed as the only plane passing through the shell that contains the logarithmic planispiral line

113 connecting the beak to a point on the ventral margin (Figure 1); all other radial lines would be

114 logarithmic turbinate spirals (or 'helicospirals'; Stasek 1963b:217). In other words, on a radially

115 ribbed shell, there may be a single rib that lies entirely on a plane when viewed from its origin at

116 the umbo to its terminus on the ventral margin; that plane is orthogonal to the commissural plane

4

117   for planispiral shells (e.g. many Pectinidae, Figure 1), but lies at increasingly acute angles to the

118   commissural plane with increasing tangential components of growth (i.e. geometric torsion; see

119   the trace of the directive plane on *Chione* in Figure 1 and examples in Cox et al. 1969:86-Figs.

120   70-71). In theory, the directive plane could be used to orient the dorsoventral axis of the shell,

121   but in practice, the feature is not universal across shell morphologies (e.g. the strongly coiled

122   *Glossus humanus* [as *Isocardia cor*] in Lison 1949:62; Owen 1952:149). Cox et al. (1969:87)

123   also remark that the plane cannot "be demonstrated easily by visual inspection if the shell lacks

124   radial ribbing, except in rare specimens with an umbonal ridge that proves to lie within the

125   directive plane." Difficulty in application is no excuse to avoid an approach, but the non-

126   universality of this feature renders it inapplicable to Class-wide comparisons of shell shape.

127   Owen (1952) proposed an alternative to the directive plane: the **demarcation line**

128   (Figure 1; originally termed the 'normal axis' but re-named by Yonge 1955:404). As with the

129   directive plane, the demarcation line serves to orient the dorsoventral direction and separate the

130   shell into anterior and posterior 'territories' (Yonge 1955:404; Morton and Yonge 1964:40), but

131   its definition has been variably characterized in geometric and/or anatomical terms. Per Owen

132   (1952:148), the demarcation line can "be considered with reference to three points: the umbo, the

133   normal zone of the mantle edge and the point at which the greatest transverse diameter of the

134   shell intersects the surface of the valves." Yonge (1955:404), acknowledging correspondence

135   with Owen, described the demarcation line as: "the projection onto the sagittal plane of the line

136   of maximum inflation of each valve … starting at the umbones. … i.e. the region where the ratio

137   of the transverse to radial component in the growth of the mantle/shell is greatest." Carter et al.

138   (2012:52) provided perhaps the clearest description as the line defining the "dorsoventral profile

139   when the shell is viewed from the anterior or posterior end." However, Stasek (1963*b*)

140   demonstrated the difficulty in measuring this line; note the nearly orthogonal orientations of the

141   empirically determined demarcation line on *Ensis* (Stasek 1963*b*:225-Fig.5a) compared to its

142   initially proposed position (Owen 1952:148-Fig. 5). Stasek's empirical approach, coupled with

143   the revised definition of Carter et al., is tractable with today's 3D-morphology toolkit. But,

144   critically, this definition depends on the direction of the anteroposterior axis, which itself is

145   variably defined (see discussion in next section). Thus, definitionally driven shifts in the

146   direction of the anteroposterior axis can alter the trace of the demarcation line. Owen's initial

147   definition is independent of the anteroposterior axis, but as Stasek demonstrated, its

148   identification can be unreliable. Thus, high degrees of digitization error for the demarcation line

149   may confound comparisons of shell shape, and we do not include the demarcation line as a

150   feature for aligning shells across the Class.

151   Both the directive plane and the demarcation line attempt to orient the shell on aspects of
152   its geometry that are intrinsic to its growth. A similar and more reliably determined approach
153   may be orientation to the **maximum growth axis** (i.e. **line of greatest marginal increment**
154   sensu Owen 1952; Figure 1). The maximum growth axis is the straight line that connects the
155   origin and terminus of the trace of maximum growth across the shell surface. This trace connects
156   the beak to the ventral margin along a perpendicular path to the most widely spaced
157   commarginal growth increments (as such, this definition appears to have similar properties to the
158   trace of the directive plane on the shell surface). But, as for the directive plane and the
159   demarcation line, the maximum growth axis can be prone to measurement error without fitting a
160   formal model of shell growth (e.g. those of Savazzi 1987; Ubukata 2003), and should therefore
161   be used with caution. However, a reasonable and reliably measured proxy for this axis is the line
162   lying on the commissural plane that originates at the beak and terminates at the furthest point on
163   the shell commissure. Thus, this axis can indicate the dorsoventral orientation of the shell.

164   Orientation using the **shape of the shell commissure** offers, arguably, the most reliably
165   determined approach that uses intrinsic properties of the shell (Figure 2a). Given the accretionary
166   growth of the shell, points on the commissure—the homologous leading edge of shell growth
167   (Vermeij 2013)—are geometrically homologous, or correspondent (Bookstein 1991; Gunz et al.
168   2005). Valve handedness is still required to ensure that compared valves are from the same side
169   of the body (i.e. left vs. right), which requires anteroposterior directionality (see below). This
170   alignment thus orients shells using geometric correspondence based on homology of growth.

171   The sagittal axis is crucial to the shell's three-dimensional alignment and is likely the
172   least controversially defined. This axis is the pole (=normal) to the sagittal plane, which lies
173   parallel to the commissural plane defined as: "the more proximal part of the line or area of
174   contact of the two shell valves" (Carter et al. 2012:38). Therefore, the sagittal axis is parallel to
175   the frontal and horizontal planes (Figure 1). The proximal direction is towards the commissural
176   plane and the distal direction is towards the shell's summit: the point on the shell that is
177   maximally distant from the commissural plane (Figure 1, Cox et al. 1969:108; Carter et al.
178   2012:177). If valve handedness (i.e. left vs. right laterality) and the directionality of the
179   dorsoventral and anteroposterior axes are known, then this axis is rarely required for orientation.
180   However, certain definitions of the anteroposterior and dorsoventral axes are not constrained to
181   be orthogonal (e.g. in monomyarian taxa with the anteroposterior axis defined as the oro-anal
182   axis, see below, and the dorsal ventral axis as the axis of maximum growth—*Pecten* in Figure 1);
183   as the axes representing the anteroposterior and dorsoventral directions become more parallel,
184   then the sagittal axis becomes an increasingly important safeguard against the inversion of the
185   proximal-distal direction in quantitative alignments.

186 **2.1.2 Orientation via the soft-body as reflected on the shell**

187 Anteroposterior directionality is the third Cartesian axis required for orienting the bivalve shell
188 in three-dimensions. The positions of the mouth (anterior) and anus (posterior) ultimately
189 determine the anteroposterior axis (Jackson 1890, 'preferably' described as the 'oro-anal' axis in
190 Cox et al. 1969:79), but the exact positions of these two soft-body features are rarely recorded
191 directly on the shell. Thus, tactics for determining the polarity, if not the precise bearing, of the
192 anteroposterior axis have relied on lineage or body-plan specific proxies—shell features that are
193 assumed to correlate with positions of the soft-body anatomy (e.g. positions of the adductor
194 muscle scars, Figure 1a, Cox et al. 1969:79). Disparate body plans necessitate taxon-specific
195 rules for orientation, such that determining the anterior and posterior ends of the shell requires a
196 mosaic approach. For example, there are at least three definitions of the anteroposterior axis in
197 dimyarians alone (Bailey 2009:493), which necessarily differ from those of monomyarians
198 considering the reliance on two, instead of one, adductor muscle scars. For those monomyarians,
199 which commonly have lost the anterior adductor (Yonge 1954; but see loss of the posterior
200 adductor in the protobranch Nucinellidae, Allen and Sanders 1969; Glover and Taylor 2013),
201 additional shell features are used to orient the anteroposterior axis. In pectinids, the byssal notch
202 of the anterior auricle proxies the location of the mouth (Figure 1b), but in ostreids, the mouth is
203 more centrally located under the umbo, near the beak (Yonge 1954:448).

204 Lineage or body-plan specific definitions help with anteroposterior orientation of shells
205 that lack point-based homology (e.g. two muscle scars vs. one), but they still rely on proxies for
206 the position of soft-body features that may not be determined for taxa known only from their
207 shells, e.g. some fossils (Bailey 2009). Hypothesizing anteroposterior orientation using
208 phylogenetic proximity to extant clades may help, but this approach should be used with caution
209 in given the lack of direct anatomical evidence—especially when phylogenetic affinities are
210 either unknown or distant, as for many Paleozoic taxa (Bailey 2009). Nor is it advisable to
211 assume the precise bearing of the anteroposterior axis is identical to another, well-defined axis
212 such as the hinge line (see variable bearings of the anteroposterior axis and hinge *axis* in Cox et
213 al. 1969:80-Fig. 64). However, if the phylogenetic or temporal scope of an analysis precludes the
214 determination of the anteroposterior axis using homologous body features with geometric
215 correspondences (e.g. inclusion of dimyarian and monomyarian taxa), then the hinge line offers a
216 universal proxy; that way, multiple features can be used to determine the anterior and posterior
217 ends of the shell (Cox et al. 1969).

2.2   Alignment of shells for geometric morphometrics

Our challenge here is to reconcile the many means of orienting bivalve shells discussed above into alignment schema for geometric morphometrics. We compare the differences in shell shape produced by the five orientations listed below. All five orientations use the sagittal axis (SX) to determine the lateral orientation of the shell. Precise definitions of landmark placement for each axis are provided in the Methods.

- **SX-HL-oHL.** Anteroposterior orientation determined by the hinge line (HL); dorsoventral orientation determined by the orthogonal line to the HL within the commissural plane (oHL). This alignment emulates the orientation scheme for measuring shell height, length, and width—the most common and widely applicable framework for comparing shell morphology (Cox et al. 1969:81–82; Kosnik et al. 2006).
- **SX-OAX-oOAX.** Anteroposterior orientation determined by the proxied positions of the mouth and anus using shell features (oro-anal axis, OAX); dorsoventral orientation determined by the orthogonal line to the OAX within the commissural plane (oOAX). Similar to SX-HL-oHL, this alignment largely determines orientation by a single axis, the OAX, which has also been used to frame linear measurements of shell morphology (e.g. Stanley 1970:19).
- **SX-HL-GX.** Anteroposterior orientation determined by the hinge line (HL); dorsoventral orientation determined by the maximum growth axis (GX). This alignment allows an aspect of shell growth to affect its orientation and thus the degrees of morphological similarity among specimens.
- **SX-HL-GX-OAX.** Anteroposterior orientation determined by the directions of both the HL and OAX; dorsoventral orientation determined by GX. This 'full' alignment scheme allows axes derived from intrinsic characteristics of the shell and the body to affect orientation.
- **SX-COMM.** Anteroposterior and dorsoventral orientation determined by the shape of the commissure curve, with the initial point nearest the beak (Figure 2a). This alignment uses the geometric correspondence of semilandmarks on the commissure that capture the relationship between its shape and growth.

Procrustes superimposition (or Procrustes Analysis) is the workhorse of geometric morphometrics—aligning shapes by translation to a common origin, scaling to common size, and rotation to minimize relative distances of landmarks (see variants thereof in Zelditch et al. 2012). While we are most concerned with assessing the effects of rotation using the five alignments described immediately above, choices of translation and scaling can also influence shape differences. Thus, we consider all combinations of parameter values for each step in the

253 Procrustes Analysis. As there is arguably no objective criterion to determine which alignment
254 best suits bivalve shells, we discuss the benefits and drawbacks of each approach and
255 quantitatively compare the similarities of resulting alignments. Ultimately, we use this exercise
256 to propose a best practice for aligning bivalve shells and comparing their shapes—a process that
257 may be of use for workers in other, similarly disparate morphological systems that lack high
258 degrees of point-based homology.

3. Methods

3.1 Dataset

261 We adopt the style of previous approaches to studying bivalve orientation and use a dataset of
262 morphological end-members to illustrate the effects of different alignment schemes (e.g. Owen
263 1952; Yonge 1954; Stasek 1963*a*). Eleven species that represent most major body plans were
264 selected to proxy the morphological and anatomical disparity across the evolutionary history of
265 the Class (Table S1). Bivalves with highly reduced shells or those that form part of a larger
266 structure (tubes and crypts) are not directly analyzed here, but we consider their fit to the
267 alignments in the Discussion.

268 One valve from an adult individual of each species was sampled from museum
269 collections (see Acknowledgments). Nine of eleven individuals are equivalve, and because we do
270 not examine details of dentition, their left and right valves are operationally mirror images of
271 each other. The inequivalve taxa included here (*Pecten*, *Ostrea*) primarily differ in terms of
272 inflation (height above the commissural plane); for the purposes of our analysis, the location of
273 key features such as the hinge area and adductor muscle scars are similar enough that using
274 either valve gives a similar orientation. Valves were scanned using micro-CT at the University of
275 Chicago's Paleo-CT facility, and three-dimensional, isosurface, triangular-mesh models were
276 created in VG Studio Max and cleaned in Rvcg (Schlager 2017) and Meshmixer. Landmarks
277 were placed using 'Pick Points' in Meshlab (Visual Computing Lab ISTI – CNR 2019). Meshes,
278 landmarks, and code necessary to reproduce the analyses here are provided in the Supplemental
279 Material.

3.2 Aligning bivalve shells in a geometric morphometrics framework

### 3.2.1 Scaling

282 Procrustes Analysis scales objects to a common size, and three alternative scalings are
283 considered here: (1) the **centroid size of the shell** (Figure 2b), (2) the **centroid size of the**
284 **commissure** (Figure 2a), and (3) the **volume of the shell**. The centroid size of the shell reflects
285 the 3D footprint of the shell, and the centroid size of the commissure reflects the size of the

286   shell's growth front. Shell volume—the amount of calcium carbonate—may be less correlated

287   with shell shape than the other two measures, and may therefore reveal shape differences not

288   intrinsically linked to size.

289   **3.2.2   Translation**

290   After scaling, Procrustes Analysis translates objects to a common origin. Objects are typically

291   'centered' by subtracting the centroid of the landmark set (mean X, Y, and Z coordinate values

292   per object) from each landmark coordinate, thus shifting the center of each landmark set to the

293   origin (X=0, Y=0, Z=0). Three points are considered for translation here: (1) the **beak** (Figure 1),

294   (2) the **centroid of the shell** (Figure 2b), and (3) the **centroid of the commissure** (Figure 2a).

295   Translation to the beak positions shells onto the homologous point of initial shell growth.

296   Translation to the centroids of the shell or its commissure incorporate more information on the

297   shape of the shell, with centering on the commissure adding an aspect of homology by

298   positioning shells on their growth front. Operationally, Procrustes Analysis translates landmark

299   sets to their respective centroids before minimizing their rotational distances, overriding any

300   prescribed translations; the three translations above are therefore implemented after the rotation

301   step (following the functionality in *Morpho::procSym* Schlager 2017).
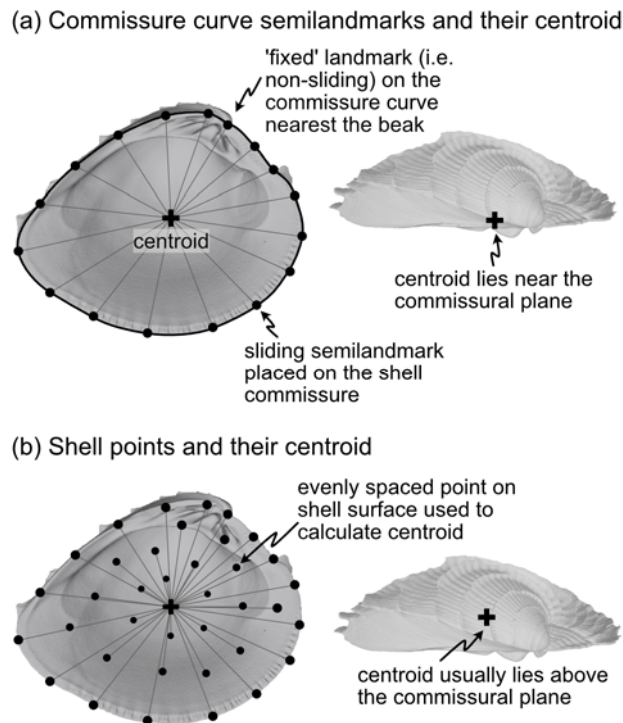
302

303   **Figure 2.** (a) Representation of shell commissure curve, its centroid, and the semilandmarks used

304   in the COMM orientation scheme. Analyses use 50 sliding semilandmarks on the commissure

305   curve, but only a subset is shown here for clarity. (b) Equally spaced points on the shell surface

306   placed using a Poisson Disc sampler (*Rvcg::vcgSample*, Schlager 2017) and their centroid. The

307   number and location of vertices on triangular meshes can vary, which strongly influences the

308   calculation of centroid size. Analyses use 2000 equally spaced points to minimize this issue

309   (only a subset of those points shown here). Figured shell is *Chione elevata*.

310   **3.2.3   Rotation**

311   Rotation in Procrustes Analysis orients landmark coordinates to minimize their pairwise sum of

312   squared distances. The 5 orientations discussed in the introduction were used for rotation.

313   Because Procrustes Analysis uses Cartesian coordinates, two landmarks were placed on the mesh

314   surface of a shell to indicate the direction of each axis as described in the subsections below

315   (exact placement of landmarks on specimens in Figure S1).

316   **Sagittal orientation**

317   *Sagittal axis [SX].* This axis is the pole to the commissural plane (Figure 1). It is determined as

318   the average cross product of successive vectors that originate at the centroid of the commissure

319   and terminate at semilandmarks on the commissure curve (visualization of fitting the

320   commissural plane in Figure S2). The distal direction is towards the exterior surface of the shell

321   and the proximal direction is towards the interior surface.

322   **Anteroposterior orientation**

323   *Hinge line [HL].* The hinge line is determined by landmarks placed at the two farthest apart

324   articulating elements of the hinge area (Figure 1). The landmarks are then designated as being

325   anterior or posterior using the available discriminating features on the shell and can thus proxy

326   the anteroposterior orientation. While not an 'axis' in the strict anatomical sense, we group the

327   hinge line with the other anatomical axes below.

328   *Oro-anal axis [OAX].* The positions of the mouth and anus or proxies thereof are used to orient

329   the oro-anal axis and thus the anteroposterior orientation. For dimyarian taxa, anterior and

330   posterior ends of the axis are determined by landmarks placed on the dorsal-most edge of the

331   anterior and posterior adductor muscle scars (Figure 1a, the 'Type 2 adductor axis' of Bailey

332   2009:493 after Stanley 1970:19). For monomyarian taxa that have retained the posterior adductor

333   muscle, the centroid of that adductor muscle scar is landmarked as the posterior end of the axis

334   and shell features that reflect the position of the mouth are landmarked as the anterior end (e.g.

335   the ventral notch of the anterior auricle in pectinids [Figure 1b] or the beak in ostreids, Yonge

336   1954). The axis is reversed in monomyarian taxa that have retained the anterior muscle (e.g. the

337   protobranch Nucinellidae, Glover and Taylor 2013).

Dorsoventral orientation

Maximum growth axis [GX]. The origin of shell growth at the beak is the dorsal landmark on the maximum growth axis and the point on the shell commissure with the greatest linear distance to the beak is ventral landmark (Figure 1).

Orthogonal hinge line [oHL]. By definition, the orthogonal line to the HL (oHL) represents the dorsoventral axis, with the dorsal-most point nearest the beak.
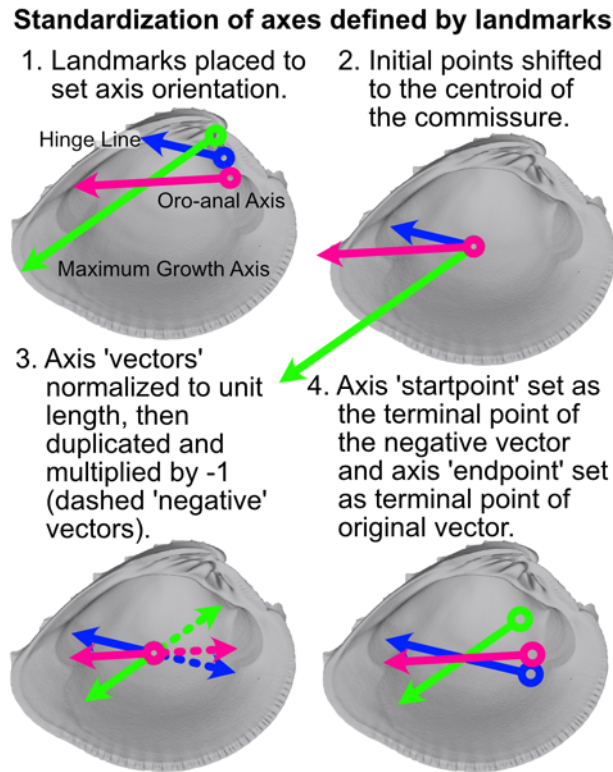
Orthogonal oro-anal axis [oAX]. By definition, the orthogonal axis to the OAX (oOAX) represents the dorsoventral axis, with the dorsal-most point nearest the beak.

Commissure orientation

The manually placed landmarks on the shell commissure were used to fit a three-dimensional spline on which 50 equally spaced semilandmarks were placed in an anterior direction (clockwise for left valves when viewed towards the interior surface, counterclockwise for right valves). The semilandmark on the commissure curve nearest the beak landmark was selected as the initial point (Figure 2a). Semilandmarks were then slid to minimize bending energy and reduce artifactual differences in shape driven by their initial, equidistant placement (Gunz et al. 2005; Gunz and Mitteroecker 2013; Schlager 2017).

Standardized axis points

We observed that variance among specimens in the distances between the axis landmarks notably influenced their best-fit orientation in the Procrustes Analysis (see difference in spacing of these landmarks in Figure S1). To remove this 'Pinocchio effect' (*sensu* Zelditch et al. 2012:67), axis landmarks were 'standardized' (visualization of this process in Figure 3). The vector defined by the two axis landmarks was shifted to the centroid of the shell commissure and normalized to unit length; the standardized axis points (we explicitly avoid calling them landmarks) were then designated by the terminal points of the unit vector and its negative. Standardized axis points result in alignments that better reflect the collective impacts of axis direction, not magnitude.

Standardization of axes defined by landmarks

1. Landmarks placed to set axis orientation.

2. Initial points shifted to the centroid of the commissure.

Hinge Line

Oro-anal Axis

Maximum Growth Axis

3. Axis 'vectors' normalized to unit length, then duplicated and multiplied by -1 (dashed 'negative' vectors).

4. Axis 'startpoint' set as the terminal point of the negative vector and axis 'endpoint' set as terminal point of original vector.

364

Figure 3. Visualization of procedure used to standardize the orientation axes defined by landmarks. Figured shell is *Chione elevata*.

3.3 Alignment and comparison of shape differences

Meshes and landmark sets for right valves were mirrored across their commissural plane and analyzed as operational left valves. This is a reasonable approach for equivalve taxa when analyzing general shell shape, e.g. of the interior or exterior surfaces, but homologous valves should be used for analyses that include inequivalve taxa as, by definition, their two shapes differ. Landmark sets were then scaled, rotated, and translated (in that order) under all possible parameter combinations outlined in the preceding section, totaling 45 alignment schemes. Landmark coordinate values were scaled by dividing the landmark coordinates by a specimen's size (e.g. centroid size or volume). Scaled landmarks were then temporarily centered on the centroid of the commissure and then rotated via the respective orientation scheme using Generalized Procrustes Analysis (*Morpho:procSym*, Schlager 2017); scaling during this step was explicitly disallowed. Lastly, scaled and rotated landmarks were translated to one of the three target locations (i.e. the beak or centroids of the commissure semilandmarks or shell points).

Similarity of alignments was quantified using the metric distances between the shapes of interior shell surfaces, which were used to reduce the impact of exterior ornamentation on the

13

382   differences in general shell shape. Sliding semilandmarks on the commissure and the interior
383   surface of the shell were used to capture 'shape.' Initially, for the commissure, 50 equidistant
384   semilandmarks were placed and the curve's starting point was determined by the orientation
385   scheme (e.g. starting at the semilandmark nearest the beak for the SX-COMM orientation, see
386   details in Supplemental Text §2.3, Figure S5); for the interior surface, semilandmarks were
387   placed at proportionate distances along the dorsoventral and anteroposterior axes of each
388   orientation scheme (5% distance used here, which results in 420 semilandmarks; see details and
389   step-by-step visualization in Supplemental Text §2.3, Figure S3, Figure S4, Figure S5). Mixing
390   the orientations of semilandmarks and rotation axes may be useful for comparing the interaction
391   of growth and anatomical direction with shell shape, but this approach can result in unintuitive,
392   and perhaps unintended, shape differences among specimens. After placement of equidistant
393   semilandmarks, those on the commissure curve were slid to minimize their thin-plate spline
394   bending energy and then used to bound the sliding of the surface semilandmarks (Figure S5;
395   Gunz et al. 2005; Gunz and Mitteroecker 2013; implemented via *Morpho::slider3d*, Schlager
396   2017). The final sliding semilandmark set consisted of 430 landmarks (50 points on the
397   commissure plus the 380 points on the surface grid which do not lie on the commissure, i.e. the
398   non-edge points; Figure S5). Landmark coverage analyses may be used at this point to maximize
399   downstream statistical power (Watanabe 2018), but we relied on qualitative assessment of shape
400   complexity and landmark coverage for the simple analyses conducted here.

401   For each of the 45 alignments, similarity in shell shape was calculated as the pairwise
402   Euclidean distances of the sliding surface semilandmarks. Identical shapes have a distance of
403   zero. Pairwise distances between shapes for each alignment scheme were normalized by their
404   respective standard deviations, making the distances between specimens comparable across
405   alignments. These normalized pairwise distances were then compared in three ways. First, a
406   permutation-based multivariate analysis of variance (perMANOVA as implemented by
407   *geomorph::procD.lm*, Adams et al. 2021) was used to model the effects of Procrustes Analysis
408   steps on the scaled pairwise distances between specimens. Each of the 45 rows in the analyzed
409   matrix was a unique Procrustes Analysis treatment, or alignment—i.e. a combination of scaling,
410   rotation, and translation—and each of the 55 columns was a scaled distance between a pair of the
411   eleven specimens. Second, this alignment matrix was scaled and centered and Principal
412   Components Analysis was conducted to visualize the individual and joint effects treatments
413   across alignments (i.e. Figure 4). Third, 'hive diagrams' (see network plots in Figure 5d) were
414   used to compare the scaled pairwise distances of specimens among selected alignments to a
415   reference alignment, where scaling = centroid of commissure, rotation = HL-oHL, translation =
416   centroid of shell commissure.

417 **4. Results and Discussion**

418 All three Procrustes Analysis steps—translation, scaling, and rotation—significantly affect the
419 alignments of shells (Table1, visualized as clustering of steps in Figure 4). As defined in the
420 Methods, quantitative similarity in alignment was determined using the scaled, pairwise
421 Euclidean distances among the sliding semilandmarks placed on the interior surface of the shell.
422 Treatments within steps (e.g. translation to the beak vs. centroid of the shell) differentiate
423 alignments while the effects of other parameters are held constant ($p=0.001$ for all parameters,
424 Table1). Scaling most strongly differentiates alignments, with rotation and translation having
425 smaller effects (see standardized effect sizes as Z scores in Table1). It follows that the
426 differences between alignments are smallest among rotation and translation treatments (i.e. the
427 smallest distances between alignments reflected as the lowest Sum of Squares, Table1, see also
428 their clustering in Figure 4), and they increase for treatments of scaling. These metric differences
429 among alignments are informative for understanding the impacts of individual steps in Procrustes
430 Analysis, but visually comparing the orientations of shells is necessary to understand an
431 alignment's fidelity to biological homology and/or analogy.

432

433 **Table 1.** Permutation multivariate analysis of variance of the scaled pairwise distances between
434 specimens across the 45 Procrustes Analysis alignments.

| Term	df	Sum of Squares	Mean Square	R^2	F	Z	p
translation	2	30.6	15.3	0.11	13.7	4.4	0.001
scaling	2	185.4	92.7	0.64	82.7	6.2	0.001
rotation	4	34.7	8.7	0.12	7.7	4.8	0.001
Residuals	36	40.3	1.1	0.14			
Total	44	291.0					

435
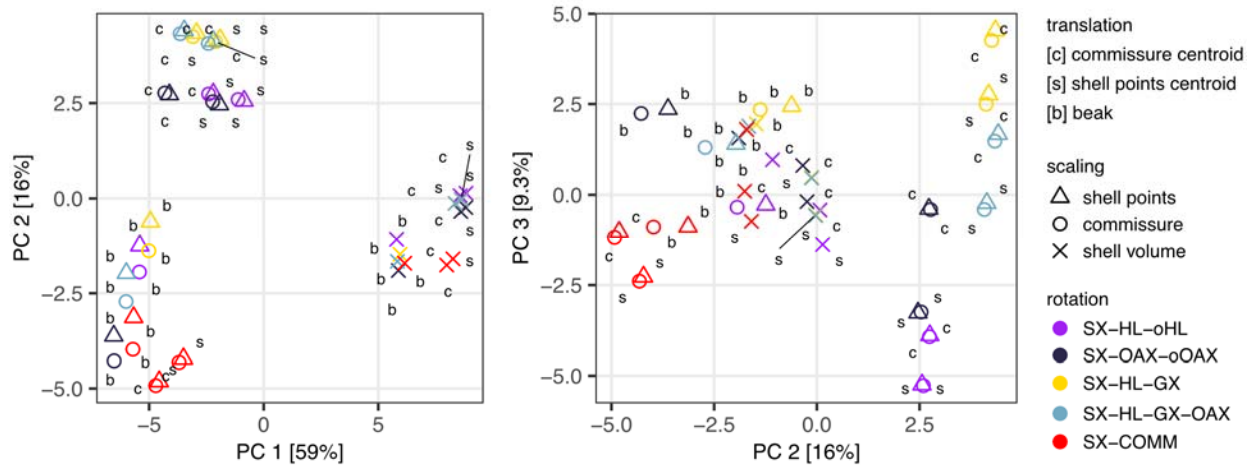
Figure 4. Principal Components Analysis of forty-five alignments (represented by points). Spacing of alignments along the first three axes that describe 84.3% of the total variance reflects the results of the MANOVA in Table1. Scaling by shell volume vs. the centroid size of either the shell points or the commissure separate along PC1; together, PCs 2 and 3 show the clustering of alignments with SX-COMM rotation, translation to the beak, the similarity of translation to the centroids of the commissure semilandmarks and shell points, and separation of the axis-based rotation schemes.

4.1 Effects of translation

The choice of translation can change how differences in shell shape are interpreted. Translation to the beak, the lone homologous point across the class, allows the comparison of shell shapes conditioned on directions of growth from their origins (Figure 5c). *Ensis* can be described as being posteriorly elongated compared to *Glycymeris*, or *Pecten* as 'taller' than *Pholas* from the beak to the ventral margin. Still, translation to the beak can exaggerate or bias the differences in 'pure' shell shape. For example, *Ensis* and *Tagelus* have greater distances between their shapes when translated to the beak than to the centroid of commissure semilandmarks (red line in Figure 5d.iii). Their offset positions of the beak underlies this difference, which is interesting for analyses of growth vs. shape, but the shape of the shell, irrespective of its growth, is arguably the primary target of ecological selection (Stanley 1970, 1975, 1988; Vermeij 2002; Seilacher and Gishlick 2014). Thus, measuring the morphological similarity of shells for studies of ecomorphology, trends in disparity, or evolutionary convergence would be best conducted using translation to their respective centroids of the commissure or shell surface (Figure 5a,b); these two translations yield very similar alignments given the close proximity of their respective centroids (as shown by the pale colors linking specimens in Figure 5d.ii; but note the small offset between the two centroids for the more irregularly shaped *Cuspidaria*). In general, it is best

16

461 practice to translate shells to their respective centroids of the commissure semilandmarks or shell
462 points when morphological analyses target differences in pure shell shape. Translation to the
463 centroid of the commissure is preferred because it incorporates homology into the alignment via
464 correspondence of the leading edge of shell growth.
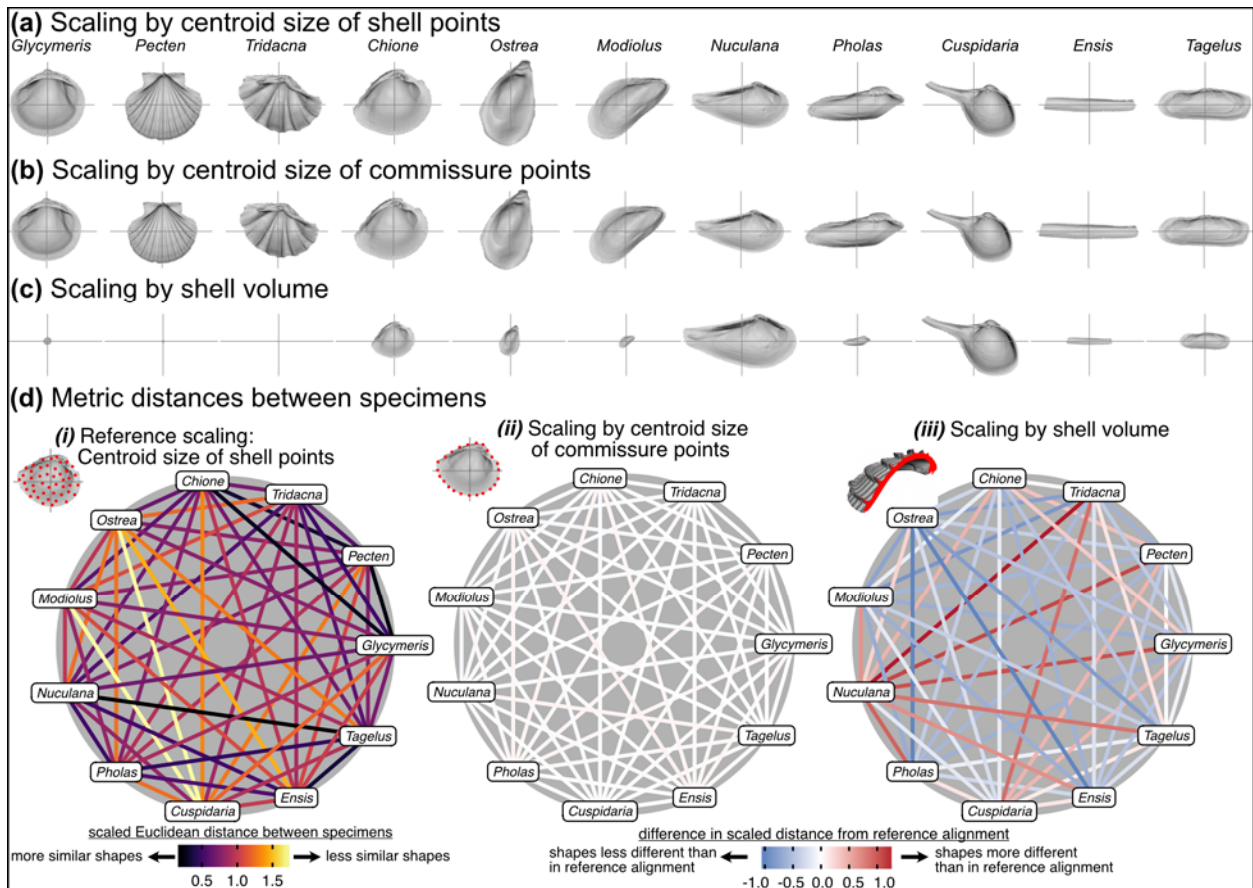
465
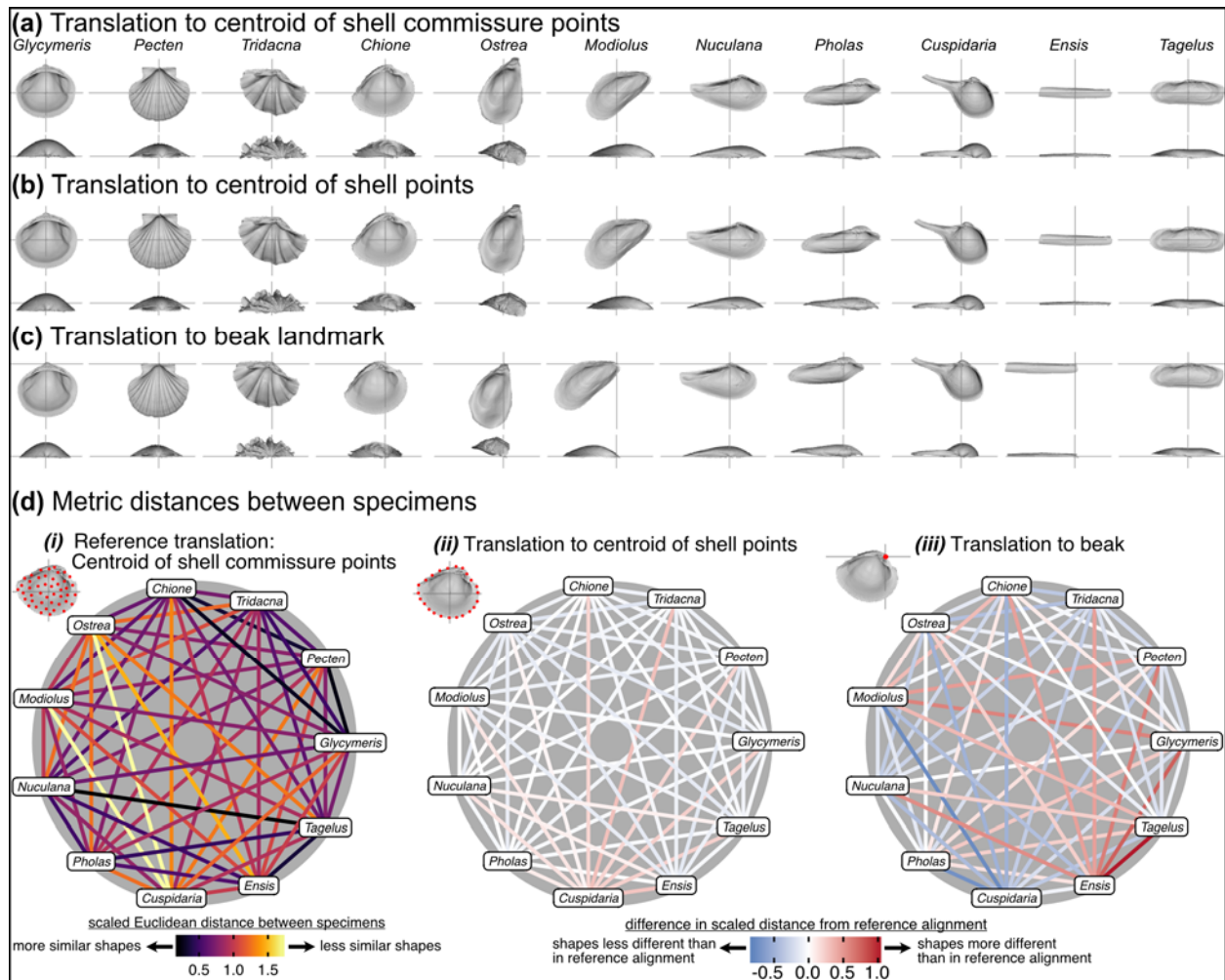
466

467 **Figure 5.** Effects of translation on differences in shell shapes. All shells are scaled to the
468 centroid size of the shell points and rotated using the SX-HL-oHL scheme. For individual images
469 of shells, the intersection of the gray line segments marks the origin of the Cartesian coordinate
470 system and thus the operational 'center' of the shell. **(a)** Translation to the centroid of the 2000
471 equidistant points placed on the mesh surface of the shell. **(b)** Translation of shells to the
472 centroid of the 50 semilandmark curve along the shell commissure. **(c)** Translation of shells to
473 the apex of the beak landmark, the initial point of shell growth. **(d)** *(i)* The scaled pairwise
474 Euclidean distances of semilandmarks placed on the interior surface of the shell, scaled to the

17

475   centroid size of the shell points and translated to the centroid of the shell commissure. 'Hotter'
476   colors indicate greater relative distances between specimens. *(ii-iii)* The difference in scaled
477   distance of specimens for the specified translation from the reference treatment in panel *i*. More
478   saturated reds indicate an increase in scaled distance relative to the reference alignment;
479   conversely, more saturated blues indicate a decrease in distance; white indicates no difference.
480   For example, *Ensis* and *Tagelus* become more dissimilar in interior shell shape when translated
481   to their respective beaks than when each are translated to their centroid of the commissure.

4.2   Effects of scaling

483   Scaling has a large effect on the differences between alignments (see largest Sum of Squares for
484   the term in the ANOVA, Table1). Scaling by volume leaves particularly large residual
485   differences in shape; the most voluminous shells are made extremely minute (*Pecten* and
486   *Tridacna* in particular, Figure 6c) while the least voluminous shells become the largest
487   (*Nuculana* and *Cuspidaria*). Scaling to logged shell volume does not alleviate these residual
488   differences (results not shown), and, moreover, the aim of this scaling step is to remove the
489   isometric relationship of size to shape, not its allometric one. The relative sizes of specimens are
490   more similar when scaled to the centroid size of the commissure semilandmarks or the shell
491   points (Figure 6a,b). These two sizes are tightly correlated (Figure S6) and thus produce very
492   similar alignments (Figure 6d.ii). For comparing differences in overall shell morphology in 3D,
493   scaling by the centroid size of shell points would best equalize the isometric differences in size
494   among specimens, thus concentrating the remaining differences in morphology to their shapes.

495
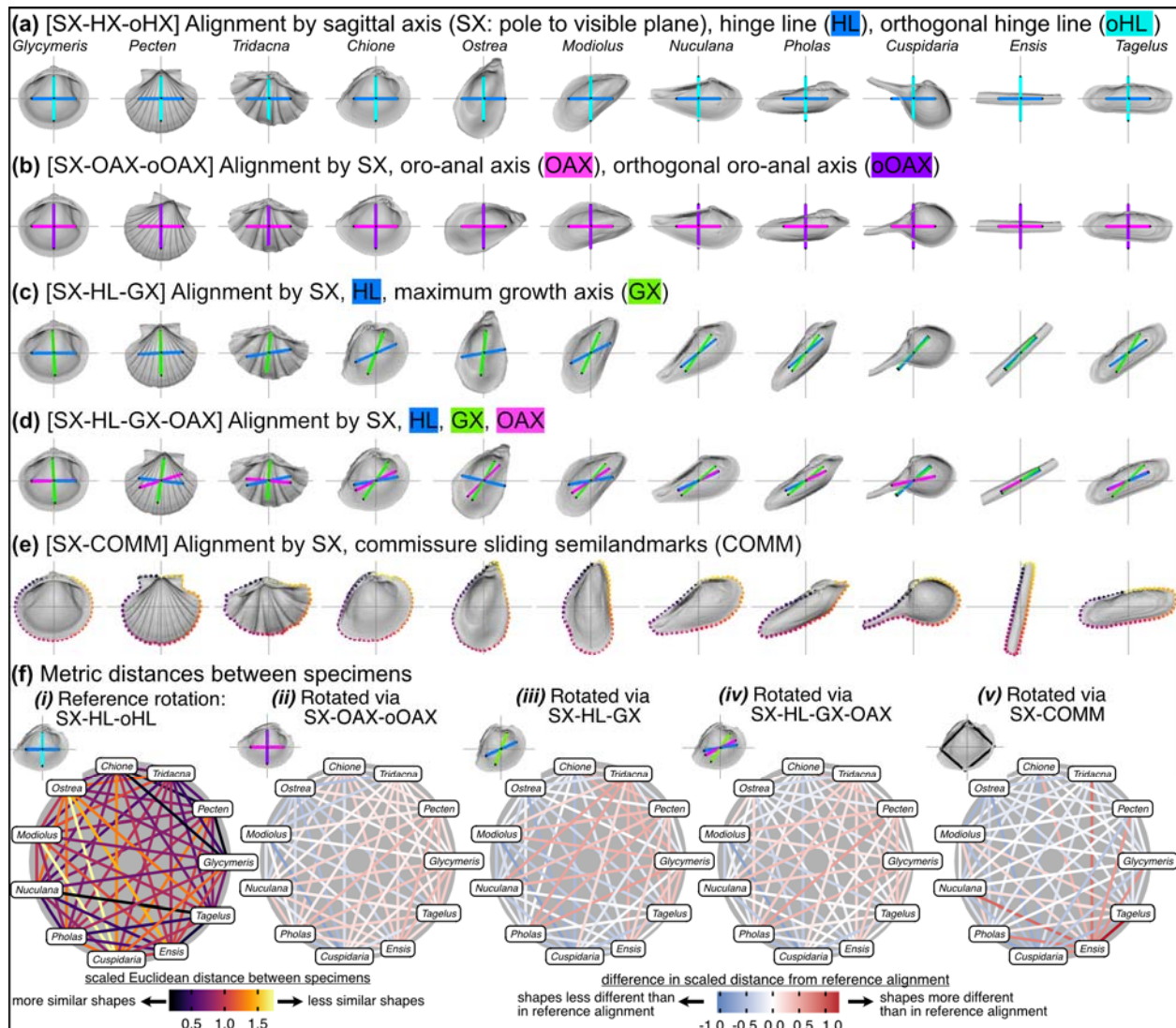
18

Figure 6. Effects of scaling on differences in shell shapes. All shells are translated centroid of the commissure semilandmarks and rotated using the SX-HL-oHL scheme. Compare differences in scaled sizes of specimens across rows, not columns. **(a)** Shells scaled by the centroid size of the 2000 equidistant points placed on the surface of the shell mesh. **(b)** Shells scaled to the centroid size of the 50 semilandmark curve along the shell commissure. **(c)** Shells scaled by the volume of shell carbonate. **(d)** As in Figure 5d but based on differences in scaling.

4.3 Effects of rotation

Of the three Procrustes Analysis parameters, rotation is arguably the most important factor defining the biological basis for differences in shell shape. Visually, rotation treatments can produce nearly orthogonal orientations of specimens (compare the nearly orthogonal orientation of the traditional shell length axis for *Ensis* and *Tagelus* between SX-HL-oHL and SX-COMM, Figure 7a,e; also reflected in the deep-red bar linking these two taxa in Figure 7f.v and is spacing of specimens on the first two PC axes in Figure S7). Equilateral shells are aligned similarly across rotation treatments (compare orientations of *Glycymeris*, *Pecten,* and *Tridacna*, cf. *Ostrea*, in Figure 7a-e and the less saturated lines connecting them in Figure 7e.ii-v). Differences in

19

512   alignments become more pronounced among the more inequilateral shells (seen to a minor extent

513   in *Chione* relative to *Glycymeris* and *Pecten*, but notably in *Modiolus, Pholas, Cuspidaria,* and

514   *Ensis*). Thus, alignments of inequilateral shells tend to reflect a compromise between the often

515   subparallel but not orthogonal orientations of their axes (most clearly seen in the changes to the

516   orientation of *Modiolus*, *Pholas*, and *Ensis* relative to *Glycymeris* and *Pecten* in Figure 7a-f).

517   Rotation by sliding semilandmarks on the commissure results in a similar alignment of most

518   shells to the hinge line orientation (pale lines in Figure 7e.v), but the relative shape differences of

519   *Modiolus*, *Ensis*, and *Tagelus* indicate the importance and impact of the beak position. The

520   commissure curve begins at the point nearest the beak, which affects the orientation of the

521   surface semilandmark grid (see Figure S5). Thus, in the SX-COMM treatment, the growth and

522   therefore 'shape' of *Modiolus* and *Ensis* is more similar to the tall-shelled *Ostrea* than either are

523   to the putative, similarly elongate *Pholas* and *Tagelus* (which themselves become more

524   dissimilar in shape owing to the slight offset in their beak positions). Overall, rotation using the

525   hinge axis and its orthogonal axis as the pseudo dorsoventral axis is likely the best practice for

526   most analyses of shell shape, as discussed below.

527

20

Figure 7. Effects of rotation on differences in shell shapes. All shells are translated centroid of the commissure semilandmarks and scaled to the centroid size of the shell points. Highlighted colors of panel titles correspond to axes plotted on shells. To facilitate relative comparisons of shell shape across columns, shells in each row were rotated such that the 'x' axis is parallel to the hinge line of *Glycymeris*; this is an ad-hoc, global rotation that does not change between-specimen differences in shell shape. **(a)** Shells rotated by their sagittal axis, hinge line, and orthogonal hinge line as the pseudo dorsoventral axis. **(b)** Shells rotated by their sagittal axis, oro-anal axis, and orthogonal oro-anal axis as the pseudo dorsoventral axis. **(c)** Shells rotated by their sagittal, hinge, and maximum growth axes. **(d)** Shells rotated by their sagittal, hinge, maximum growth, and oro-anal axes **(e)** Shells rotated by their sagittal axis and commissure

539   semilandmarks. **(f)** As in Figure 5d but based on differences in rotation. See Figure S7 for a
540   projection of shell shape differences along the first two principal components.

4.4   Practical alignments for bivalve shells

542   The axis-based approach to alignment (Figure 7a-d) is useful both for its ability to
543   encompass broad phylogenetic analyses of shell morphology and for its ability to combine extant
544   and fossil data, the latter known almost exclusively from shells. All shell morphologies should fit
545   within this scheme, including those with strong lateral asymmetry (e.g. rudists, see Jablonski
546   2020, and those with calcified tubes or crypts (teredinids and clavagellids, Morton 1985; Savazzi
547   1999, each of which have identifiable valves with anatomical axes—whether to include the tubes
548   and crypts as aspects of shell morphology is a different debate). With increasing phylogenetic
549   proximity, the number of point-based biological homologies is likely to increase, permitting
550   more traditional approaches to specimen alignment (Roopnarine 1995; Roopnarine et al. 2008;
551   Márquez et al. 2010; Serb et al. 2011; Collins et al. 2013, 2020; Edie et al. 2022; Milla Carmona
552   et al. First View). These shell-based axes and features (Figure 7a-e) are also useful for
553   incorporating fossil taxa into analyses with extant taxa (Yonge 1954; Cox et al. 1969; Stanley
554   1970; Bailey 2009), but aspects of the internal anatomy remain crucial for orientation (Stasek
555   1963*a*), especially the designation of the anterior and posterior ends. Fortunately, in many cases
556   the anteroposterior axis can be determined from imprints of the soft anatomy on the shell surface
557   (e.g. the pallial sinus) or from other shell features (e.g. siphonal canals, pedal gapes). This
558   necessarily variable and often idiosyncratic approach to defining the direction of anatomical axes
559   may result in more digitization error than seen in traditional point-based geometric
560   morphometrics. However, the impact of that error on analytical interpretations of shape
561   similarity and variance will depend on the overall scale of shape disparity; for analyses of
562   morphology across the class, the latter is likely to far exceed the former.

563   In biological systems with limited homology in a strict, point-based, geometric sense—
564   and even in those with plenty of it—numerous approaches have been used to align specimens for
565   morphological analysis. A single solution likely does not exist, and comparisons among different
566   methods will be the most powerful approach to testing evolutionary hypotheses (see Bromham
567   2016 for the necessity of comparative analyses in historical science). As for most analytical
568   frameworks, comparisons of shell shape will require explicit definition of the alignment scheme
569   and interpretation of any differences within those boundaries. Thus, we cannot declare outright
570   that one of these alignment schemes is logically superior, but we do recognize a practical
571   solution that, to us, best reflects the decades of study of shell morphology: alignment via the
572   sagittal axis, hinge line, and its orthogonal line as the pseudo dorsoventral axis (SX-HL-oHL).
573   Shell height, length, and width have been the principal measurements for analyzing differences

574 in shape, and long-standing, taxon-specific 'rules' have become entrenched in the literature and
575 therefore influence our interpretations of the clade's evolutionary morphology (see discussion in
576 Cox et al. 1969:81–82 and the continued utility of these measurements in Kosnik et al. 2006).
577 The SX-HL-oHL rotation tends to orient shells according to the defined axes of those linear
578 measurements. Of course, precedent need not dictate the course of future work, but here, we find
579 it reasonable to align this 'next generation' of shell shape analyses with the long-standing
580 conventions in the literature, if only for comparative purposes.

5. Conclusions

582 The debate on how to align specimens is still relevant in the current era of morphometry, where
583 comparisons of animal form are increasingly accessible in 2D, 3D, and even 4D (Boyer et al.
584 2016; Olsen et al. 2017; Pearson et al. 2020). But, no matter how shapes are compared,
585 interpretations of their differences or variances should be with respect to an assumed anatomical
586 alignment. For comparisons of disparate morphologies, particularly those that lack biological
587 homology conducive to point-based landmarking, alignments will likely require non-standard
588 approaches so that shape differences do not depend on geometric correspondence alone. In
589 bivalves, anatomical axes inferred from taxon-specific features offer a class-wide approach to
590 orientation. One set of axes in particular (HL-SX-DVX) coincides with historical approaches to
591 their morphometry, while another offers new insight into the relationship between shell shape
592 and shell growth (COMM-SX). Either of these solutions are valid in their own way. This
593 philosophy of specimen alignment may be particularly relevant to other model systems in
594 paleobiology and macroevolution that have accretionary-style growth: gastropods, brachiopods,
595 corals, bryozoans, etc.—each with limited point-based landmarks corresponding to biological
596 homology.

6. Acknowledgments

7. Funding

8. Data Availability

604 Mesh models, landmark data, and code for reproducing analyses and figures available from
605 Zenodo: 10.5281/zenodo.6326531.

9. Authors' contributions

SME and KSC designed the study, SME performed analyses, all authors contributed to the writing.

10. References

Adams, D. C., M. L. Collyer, A. Kaliontzopoulou, and E. K. Baken. 2021: Geomorph: Software for geometric morphometric analyses. R package version 4.0. https://cran.r-project.org/web/packages/geomorph/index.html

Allen, J. A., and H. L. Sanders. 1969: *Nucinella serrei* Lamy (Bivalvia: Protobranchia), A monomyarian solemyid and possible living actinodont. Malacologia 7:381–396.

Bailey, J. B. 2009: Shell orientation terminology among the Bivalvia (Mollusca): Problems and proposed solutions. Journal of Paleontology 83:493–495.

Bardua, C., R. N. Felice, A. Watanabe, A.-C. Fabre, and A. Goswami. 2019: A practical guide to sliding and surface semilandmarks in morphometric analyses. Integrative Organismal Biology 1:obz016.

Bookstein, F. L. 1991: Landmarks. Pp. 55–87 *in* Morphometric Tools for Landmark Data: Geometry and Biology. Cambridge University Press, Cambridge.

Borras, A., J. Pascual, and J. C. Senar. 2000: What do different bill measures measure and what is the best method to use in granivorous birds? Journal of Field Ornithology 71:606–611.

Boyer, D. M., G. F. Gunnell, S. Kaufman, and T. M. McGeary. 2016: Morphosource: Archiving and sharing 3-D digital specimen data. The Paleontological Society Papers 22:157–181.

Bradshaw, J. D., and M. A. Bradshaw. 1971: Functional morphology of some fossil palaeotaxodont bivalve hinges as a guide to orientation. Palaeontology 14:242–249.

Bromham, L. 2016: Testing hypotheses in macroevolution. Studies in History and Philosophy of Science Part A 55:47–59.

Carter, J. G., P. J. Harries, N. Malchus, A. F. Sartori, L. C. Anderson, R. Bieler, A. E. Bogan, E. V. Coan, J. C. W. Cope, S. M. Cragg, J. R. García-March, J. Hylleberg, P. Kelley, K. Kleemann, C. McRoberts, P. M. Mikkelsen, J. Pojeta, W. Skelton, I. Tëmkin, T. Yancey, and A. Zieritz. 2012: Illustrated glossary of the Bivalvia. Treatise Online No. 48, Part N, Revised, Volume 1, Chapter 31:1–209.

Carter, R. M. 1967: On the nature and definition of the lunule, escutcheon and corcelet in the Bivalvia. Journal of Molluscan Studies 37:243–263.

Collins, K. S., J. S. Crampton, and M. Hannah. 2013: Identification and independence: Morphometrics of Cenozoic New Zealand *Spissatella* and *Eucrassatella* (Bivalvia, Crassatellidae). Paleobiology 39:525–537.

640   Collins, K. S., S. M. Edie, and D. Jablonski. 2020: Hinge and ecomorphology of *Legumen*
641   Conrad, 1858 (Bivalvia, Veneridae), and the contraction of venerid morphospace
642   following the end-Cretaceous extinction. Journal of Paleontology 94:489–497.

643   Cox, L. R., C. P. Nuttall, and E. R. Trueman. 1969: General features of Bivalvia. Pp. 2–129 *in* R.
644   C. Moore, ed. Treatise of Invertebrate Paleontology. Part N, Mollusca 6, Bivalvia. Vol. 1.
645   Geological Society of America & University of Kansas, Boulder, CO & Lawrence, KS.

646   Crame, J. A. 2020: Early Cenozoic evolution of the latitudinal diversity gradient. Earth-Science
647   Reviews 202:103090.

648   Edie, S. M., D. Jablonski, and J. W. Valentine. 2018: Contrasting responses of functional
649   diversity to major losses in taxonomic diversity. Proceedings of the National Academy of
650   Sciences U.S.A. 115:732–737.

651   Edie, S. M., S. C. Khouja, K. S. Collins, N. M. A. Crouch, and D. Jablonski. 2022: Evolutionary
652   modularity, integration and disparity in an accretionary skeleton: Analysis of venerid
653   Bivalvia. Proceedings of the Royal Society B: Biological Sciences 289:20211199.

654   Fang, Z., and T. M. Sanchez. 2012: Origin and early evolution of the Bivalvia. Treatise Online
655   no. 43: Part N, Revised, Volume 1, Chapter 16:1–21.

656   Glover, E. A., and J. D. Taylor. 2013: A new shallow water species of *Nucinella* from the
657   Philippines (Bivalvia: Protobranchia: Nucinellidae), member of a tropical seagrass
658   chemosynthetic community. The Nautilus 127:101–106.

659   Gunz, P., and P. Mitteroecker. 2013: Semilandmarks: A method for quantifying curves and
660   surfaces. Hystrix, the Italian Journal of Mammalogy 24:103–109.

661   Gunz, P., P. Mitteroecker, and F. L. Bookstein. 2005: Semilandmarks in three dimensions. Pp.
662   73–98 *in* D. E. Slice, ed. Modern Morphometrics in Physical Anthropology. Kluwer
663   Academic Publishers-Plenum Publishers, New York.

664   Jablonski, D. 2020: Developmental bias, macroevolution, and the fossil record. Evolution &
665   Development 22:103–125.

666   Jablonski, D., S. Huang, K. Roy, and J. W. Valentine. 2017: Shaping the latitudinal diversity
667   gradient: New perspectives from a synthesis of paleobiology and biogeography.
668   American Naturalist 189:1–12.

669   Jackson, R. T. 1890: Phylogeny of the Pelecypoda: The Aviculidae and their allies. Memoirs of
670   the Boston Society of Natural History 4:277–400.

671   Kosnik, M. A., D. Jablonski, R. Lockwood, and P. M. Novack-Gottshall. 2006: Quantifying
672   molluscan body size in evolutionary and ecological analyses: Maximizing the return on
673   data-collection efforts. PALAIOS 21:588–597.

674   Lison, L. 1949: Recherches sur la forme et la mécanique de développement des coquilles des
675   Lamellibranches. Mémoires Institut royal des Sciences Naturelles de Belgique 34:3–87.

676 Marin, F., N. Le Roy, and B. Marie. 2012: The formation and mineralization of mollusk shell.
677   Frontiers in Bioscience (Schol. Ed.) S4:1099–1125.

678 Márquez, F., R. Amoroso, M. Gowland Sainz, and S. Van der Molen. 2010: Shell morphology
679   changes in the scallop *Aequipecten tehuelchus* during its life span: A geometric
680   morphometric approach. Aquatic Biology 11:149–155.

681 Mikkelsen, P. M., R. Bieler, I. Kappner, and T. A. Rawlings. 2006: Phylogeny of Veneroidea
682   (Mollusca: Bivalvia) based on morphology and molecules. Zoological Journal of the
683   Linnean Society 148:439–521.

684 Milla Carmona, P. S., D. G. Lazo, and I. M. Soto. First View: Ontogeny in the steinmanellines
685   (Bivalvia: Trigoniida): An intra- and interspecific appraisal using the Early Cretaceous
686   faunas from the Neuquén Basin as a case study. Paleobiology.

687 Morton, B. 1985: Adaptive radiation in the Anomalodesmata. Pp. 405–459 *in* The Mollusca,
688   Vol. 10, Evolution. Elsevier.

689 Morton, J. E., and C. M. Yonge. 1964: Classification and structure of the Mollusca. Pp. 1–58 *in*
690   K. M. Wilbur and C. M. Yonge, eds. Physiology of Mollusca. Vol. 1. Elsevier, New
691   York.

692 Olsen, A. M., A. L. Camp, and E. L. Brainerd. 2017: The opercular mouth-opening mechanism
693   of largemouth bass functions as a 3D four-bar linkage with three degrees of freedom.
694   Journal of Experimental Biology 220:4612–4623.

695 Owen, G. 1952: Shell-form in the Lamellibranchia. Nature 170:148–149.

696 Pearson, K. D., G. Nelson, M. F. J. Aronson, P. Bonnet, L. Brenskelle, C. C. Davis, E. G. Denny,
697   E. R. Ellwood, H. Goëau, J. M. Heberling, A. Joly, T. Lorieul, S. J. Mazer, E. K.
698   Meineke, B. J. Stucky, P. Sweeney, A. E. White, and P. S. Soltis. 2020: Machine learning
699   using digitized herbarium specimens to advance phenological research. BioScience
700   70:610–620.

701 Polly, P. D., and N. MacLeod. 2008: Locomotion in fossil carnivora: An application of
702   eigensurface analysis for morphometric comparison of 3D surfaces. Palaeontologia
703   Electronica 11:1–13.

704 Roopnarine, P. D. 1995: A re-evaluation of evolutionary stasis between the bivalve species
705   *Chione erosa* and *Chione cancellata* (Bivalvia: Veneridae). Journal of Paleontology
706   69:280–287.

707 Roopnarine, P. D., J. Signorelli, and C. Laumer. 2008: Systematic, biogeographic, and
708   microhabitat-based morphometric variation of the bivalve *Anomalocardia squamosa*
709   (Bivalvia: Veneridae: Chioninae) in Thailand. The Raffles Bulletin of Zoology 18:90–98.

710 Savazzi, E. 1987: Geometric and functional constraints on bivalve shell morphology. Lethaia
711   20:293–306.

26

712   Savazzi, E. 1999: Borng, nestling and tube-dwelling bivalves. Pp. 205–237 *in* Functional
713   Morphology of the Invertebrate Skeleton. John Wiley & Sons, Chichester.
714   Scarlato, O. A., and Y. I. Starobogatov. 1978: Phylogenetic relations and the early evolution of
715   the Class Bivalvia. Philosophical Transactions of the Royal Society B: Biological
716   Sciences 284:217–224.
717   Schlager, S. 2017: Morpho and Rvcg – Shape analysis in R: R-Packages for geometric
718   morphometrics, shape analysis and surface manipulations. Pp. 217–256 *in* G. Zheng, S.
719   Li, and G. Székely, eds. Statistical Shape and Deformation Analysis: Methods,
720   Implementation and Applications. Academic Press, London, UK.
721   Seilacher, A., and A. D. Gishlick. 2014: Morphodynamics. CRC Press, Boca Raton, FL.
722   Serb, J. M., A. Alejandrino, E. Otárola-Castillo, and D. C. Adams. 2011: Morphological
723   convergence of shell shape in distantly related scallop species (Mollusca: Pectinidae).
724   Zoological Journal of the Linnean Society 163:571–584.
725   Stanley, S. M. 1970: Relation of shell form to life habits of the Bivalvia (Mollusca). Geological
726   Society of America Memoirs 125:1–282.
727   ———. 1975: Why clams have the shape they have: An experimental analysis of burrowing.
728   Paleobiology 1:48–58.
729   ———. 1988: Adaptive morphology of the shell in bivalves and gastropods. Pp. 105–141 *in* E.
730   R. Trueman and M. R. Clarke, eds. The Mollusca Vol. 11, Form and Function. Academic
731   Press, San Diego.
732   Stasek, C. R. 1963a: Orientation and form in the bivalved Mollusca. Journal of Morphology
733   112:195–214.
734   Stasek, C. R. 1963b: Geometrical form and gnomonic growth in the bivalved Mollusca. Journal
735   of Morphology 112:215–231.
736   Taylor, J. D., and E. Glover. 2021: Biology, Evolution and Generic Review of the
737   Chemosymbiotic Bivalve Family Lucinidae. Series 182, The Ray Society, London, UK.
738   Trueman, E. R. 1964: Adaptive morphology in palaeoecological interpretation. Pp. 45–74 *in* J.
739   Imbrie and N. D. Newell, eds. Approaches to Paleontology. Wiley, New York.
740   Ubukata, T. 2003: Pattern of growth rate around aperture and shell form in Bivalvia: A
741   theoretical morphological study. Paleobiology 29:480–491.
742   Vermeij, G. J. 2002: Characters in context: Molluscan shells and the forces that mold them.
743   Paleobiology 28:41–54.
744   Vermeij, G. J. 2013: Molluscan marginalia: Hidden morphological diversity at the bivalve shell
745   edge. Journal of Molluscan Studies 79:283–295.
746   Visual Computing Lab ISTI – CNR. 2019: Meshlab. https://www.meshlab.net
747   Waller, T. R. 1998: Origin of the molluscan class Bivalvia and a phylogeny of major groups. Pp.

748   1–45 *in* P. Johnston and J. Haggart, eds. Bivalves: An Eon of Evolution. Vol. 1.
749   University of Calgary Press, Calgary.

750   Watanabe, A. 2018: How many landmarks are enough to characterize shape and size variation?
751   PLOS ONE 13:e0198341.

752   Yonge, C. M. 1954: The monomyarian condition in the Lamellibranchia. Transactions of the
753   Royal Society of Edinburgh 62:443–478.

754   Yonge, C. M. 1955: Adaptation to rock boring in *Botula* and *Lithophaga* (Lamellibranchia,
755   Mytilidae) with a discussion on the evolution of this habit. Quarterly Journal of
756   Microscopical Science 96:383–410.

757   Zelditch, M. L., D. L. Swiderski, and H. D. Sheets. 2012: Geometric Morphometrics for
758   Biologists: A Primer. 2nd ed. Academic Press, San Diego, CA.

759

28

760 **Supplemental Material**

761 **S1. Supplemental Data**

762 Table S1. Taxa used in this study and source of material.

family	genus	species	authority	valve	museum	catalog no.	biv3d.meshid
Cardiidae	*Tridacna*	*squamosa*	(Lamarck 1819)	L	FMNHIZ	166020	317
Cuspidariidae	*Cuspidaria*	*rostrata*	(Spengler 1793)	L	USNM	811161	1272
Glycymerididae	*Glycymeris*	*glycymeris*	(Linnaeus 1758)	L	USNM	199801	1683
Mytilidae	*Modiolus*	*modiolus*	(Linnaeus 1758)	R	FMNHIZ	126621	570
Nuculanidae	*Nucula*	*pernula*	(Mueller 1779)	L	BMNH	20180321	3255
Ostreidae	*Ostrea*	*capsa*	J. G. F. Fischer von Waldheim 1807	R	FMNHIZ	279417	138
Pectinidae	*Pecten*	*maximus*	(Linnaeus 1767)	R	USNM	25529	1566
Pholadidae	*Pholas*	*dactylus*	Linnaeus 1758	L	USNM	337277	2380
Solecurtidae	*Tagelus*	*plebeius*	(Lightfoot 1786)	L	FMNHIZ	177579	769
Solenidae	*Ensis*	*siliqua*	(Linnaeus 1758)	L	USNM	27141	3144
Veneridae	*Chione*	*elevata*	(Say 1822)	L	FMNHIZ	176349	180

763   **S2. Supplemental Methods**

764   **S2.1. Placement of axis landmarks**
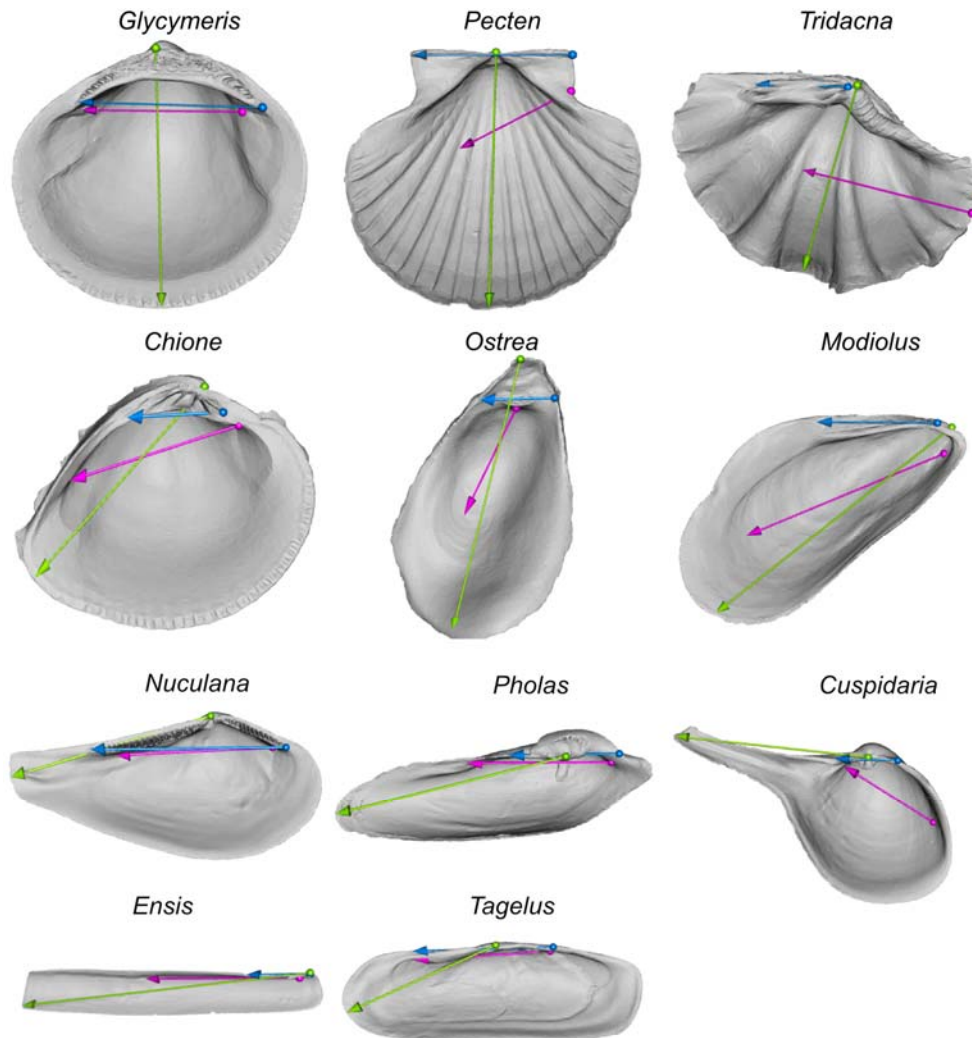
765

766   **Figure S1.** Placement of landmarks for axes (blue = hinge line; green = growth axis; magenta =
767   oro-anal axis). Origins of axis vectors as spheres, termini as arrowheads. For the hinge line and
768   oro-anal axis, spheres are anterior and arrowheads are posterior. For the growth axis, spheres
769   mark the beak and arrowhead the farthest linear distance from the beak to a point on the
770   commissure.

S2.2. Fitting the commissural plane

1. Equidistant landmarks sampled around commissure (black points). Centroid of commissure points determined (red point).

2. Determine cross product of successive vectors that start at the centroid of the commissure and end at successive points on the commissure. One example shown here.

3. Resulting normal vectors across the commissure.

4. Find mean normal vector and use as pole to the plane defining commissural plane. Plane may not rest strictly on the edges of the commissure if gapes are present, as is the case for this valve of *Pholas*.
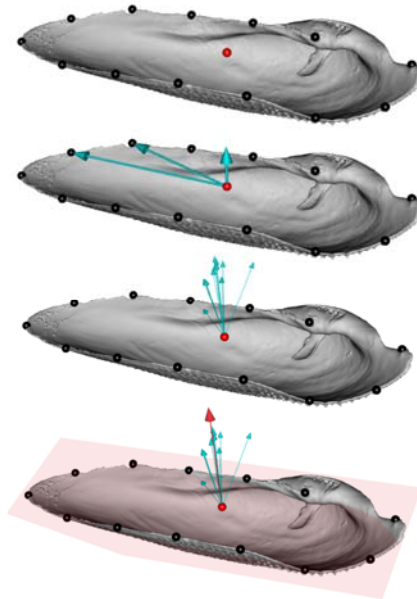
Figure S2. Visualization of procedure for fitting the commissural plane.

S2.3. Landmarking the interior surface of the shell

First, the triangular surface mesh of the shell is 'cut' into two pieces using the commissure curve: (1) interior (facing the commissural plane, or proximally directed on the sagittal axis) and (2) exterior (facing away from the commissural plane, or distally directed on the sagittal axis); visualization and step-by-step details in Figure S3.

Then, equidistant surface semilandmarks are placed on the 'interior' surface of the shell mesh as described in Figure S4 (inspired by the eigensurface method of Polly and MacLeod 2008). Note that in Figure S4-Step 5, sorting points on a flat surface best handles the ordering of points on the often topographically complex and recurved surfaces, which, in our experience, confound sorting in three-dimensions. This process is imperfect, but, again, in our experience, more reliably captures the morphology of shell surfaces compared to atlas-based approaches (Schlager 2017; Bardua et al. 2019). Bardua et al. (2019:22) state: "more accurate placement of surface points is a far more biologically sound characterization of morphology than spurious placement"—which is why we used the gridded approach in Figure S4 to place the initial semilandmarks. After placement, the equidistant semilandmarks on each individual are slid to minimize their thin-plate spline (TPS) bending energy to the mean Procrustes shape (Gunz et al. 2005; Gunz and Mitteroecker 2013; implemented via *Morpho::slider3d* Schlager 2017). The

791   start point of the commissure curve and the orientation of the surface semilandmark grid depend
792   on the orientation scheme:

793   ● For the commissure orientation (SX-COMM), the initial and 'fixed' (i.e. non-sliding)
794   point of the 50-point, equidistant commissure curve is the point nearest the beak
795   (Figure S5e). The other 49 semilandmarks along the commissure curve are then slid to
796   minimize their TPS bending energy. The surface semilandmark grid is laid down at 5%
797   distances along an arbitrary sampling axis that spans the 13th and 38th sliding
798   semilandmarks on the commissure curve, which generally reflect the anterior and
799   posterior directions, respectively. The outermost grid points that intersect the commissure
800   of the valve are removed because they will be replaced by the sliding commissure
801   semilandmarks in the final set. The semilandmark grid is then slid to minimize its TPS
802   bending energy, using the sliding semilandmarks on the commissure curve to constrain
803   the sliding of the surface semilandmarks. All sliding semilandmarks are constrained to lie
804   on the mesh surface. Thus, the final landmark set consists of 50 sliding semilandmarks
805   along the commissure and 380 sliding semilandmarks on the interior surface of the shell,
806   totaling 430 sliding semilandmarks.
807   ● For the oro-anal axis orientation (SX-OAX-oOAX), the initial and 'fixed' point of the 50-
808   point, equidistant commissure curve is the point that forms the smallest angle between the
809   orthogonal oro-anal axis vector and a vector originating at the centroid of the commissure
810   curve and terminating at a point along it (Figure S5b). The aim is to reduce the impact of
811   the beak position on the shape of the shell, that is, to remove the effects of shell growth
812   on comparisons on its shapes. The sampling axis for the surface semilandmarks is the
813   oro-anal axis. The commissure curve and surface semilandarks are slid as above.
814   ● For the orientations that include the hinge line (SX-HL-oHL, SX-HL-GX, and SX-HL-
815   GX-OAX), the initial and 'fixed' point of the 50-point, equidistant commissure curve is
816   the point that forms the smallest angle between the orthogonal hinge line vector and a
817   vector originating at the centroid of the commissure curve and terminating at a point
818   along it (Figure S5a,c,d). The aim is the same as for the oro-anal axis above, and the
819   semilandmarks are slid as in the SX-COMM case above.

820

32

1. Landmark the shell commissure. Points are ordered counter-clockwise, starting at the point nearest the beak. Manually placed landmarks are upsampled to 250 equally spaced points using a 3D-spline.

2. Use Dijkstra's algorithm to determine the shortest path between vertices on the mesh nearest the commissure landmarks (blue line connected edges on mesh between the green points).
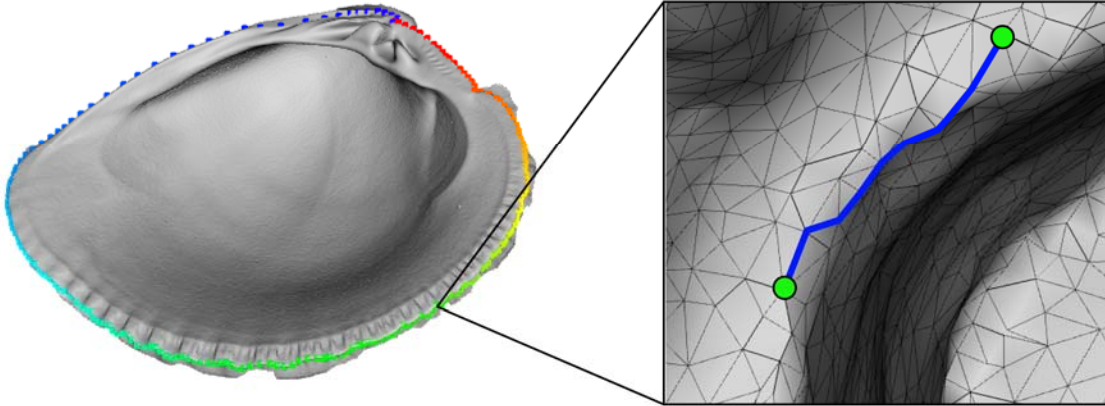
3. Temporarily remove faces from the mesh that contain the vertices connecting the blue line. This separates the mesh into two parts, which can then be partitioned into interior (gray) and exterior (orange) meshes.

4. Once separated, the temporarily removed faces along the commissure are added back to both meshes to make the 'cut' seamless.
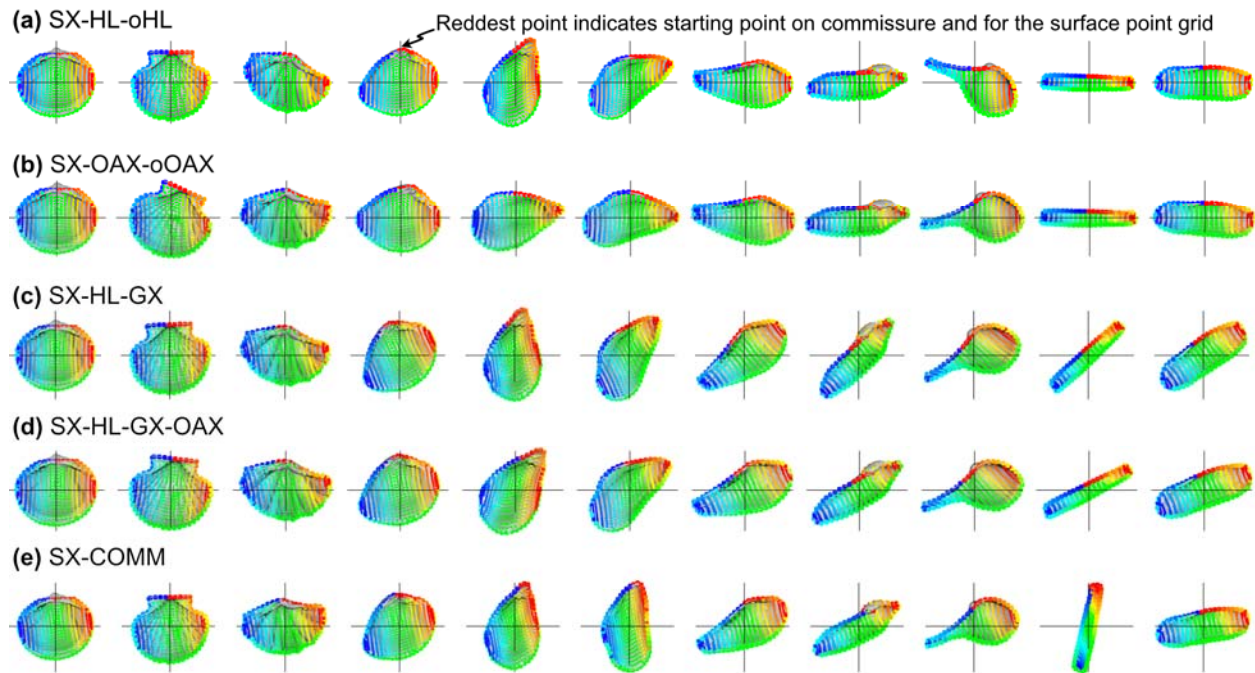
interior surface

exterior surface

821
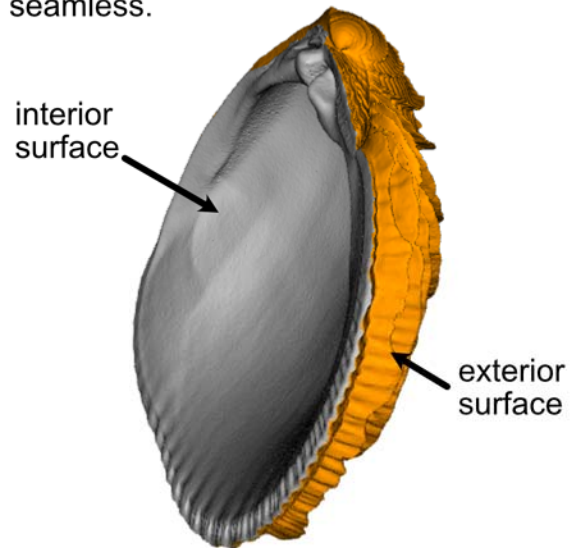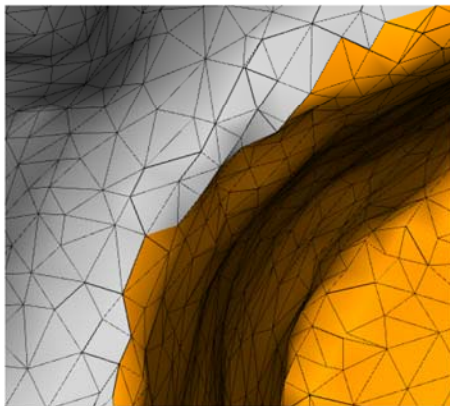
Figure S3. Visualization of the process for separating, or 'cutting,' shell meshes into interior and exterior surfaces.

33
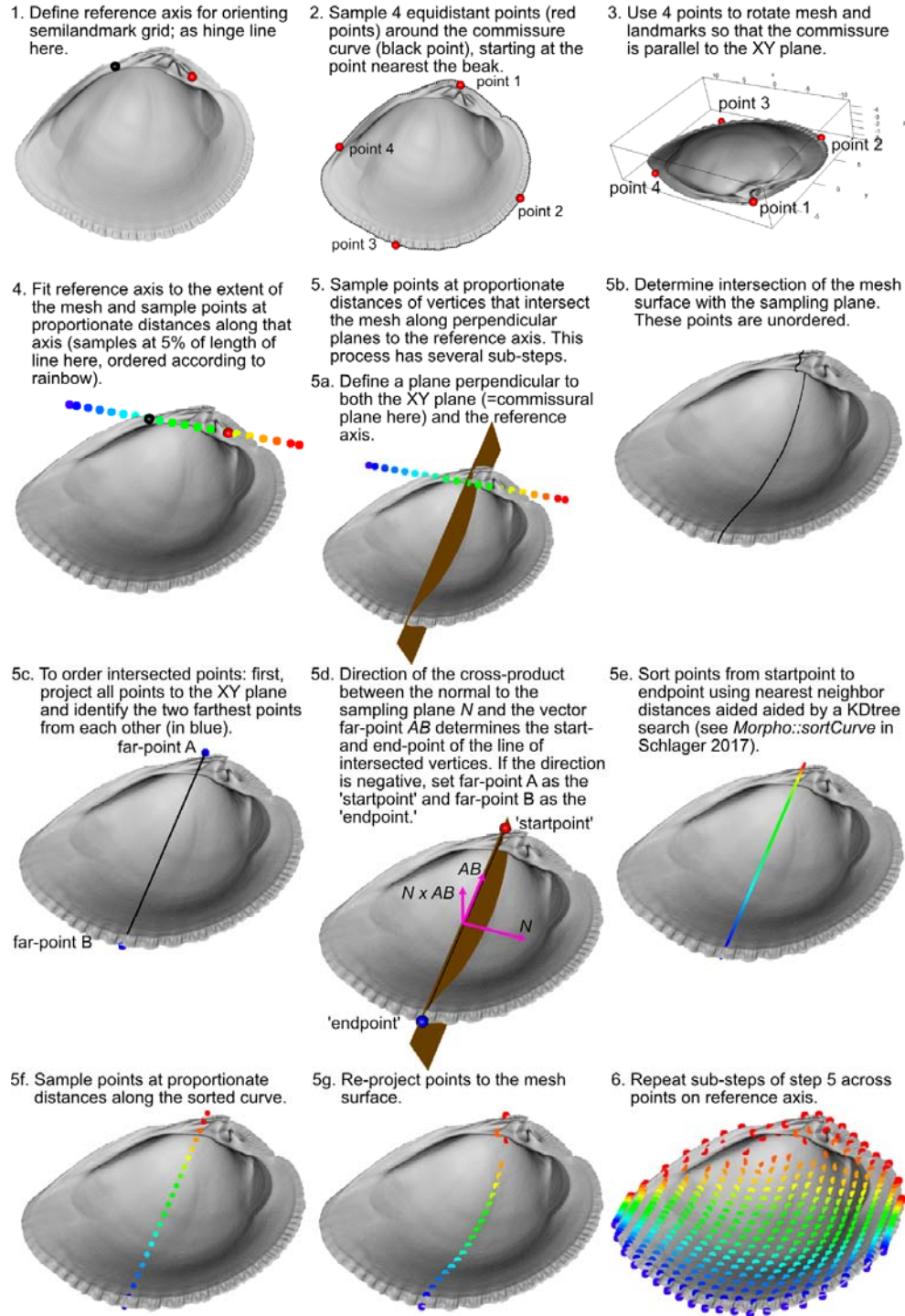
824

825 **Figure S4.** Visualization of the process for placing equidistant surface semilandmarks on the
826 interior surface of the shell.

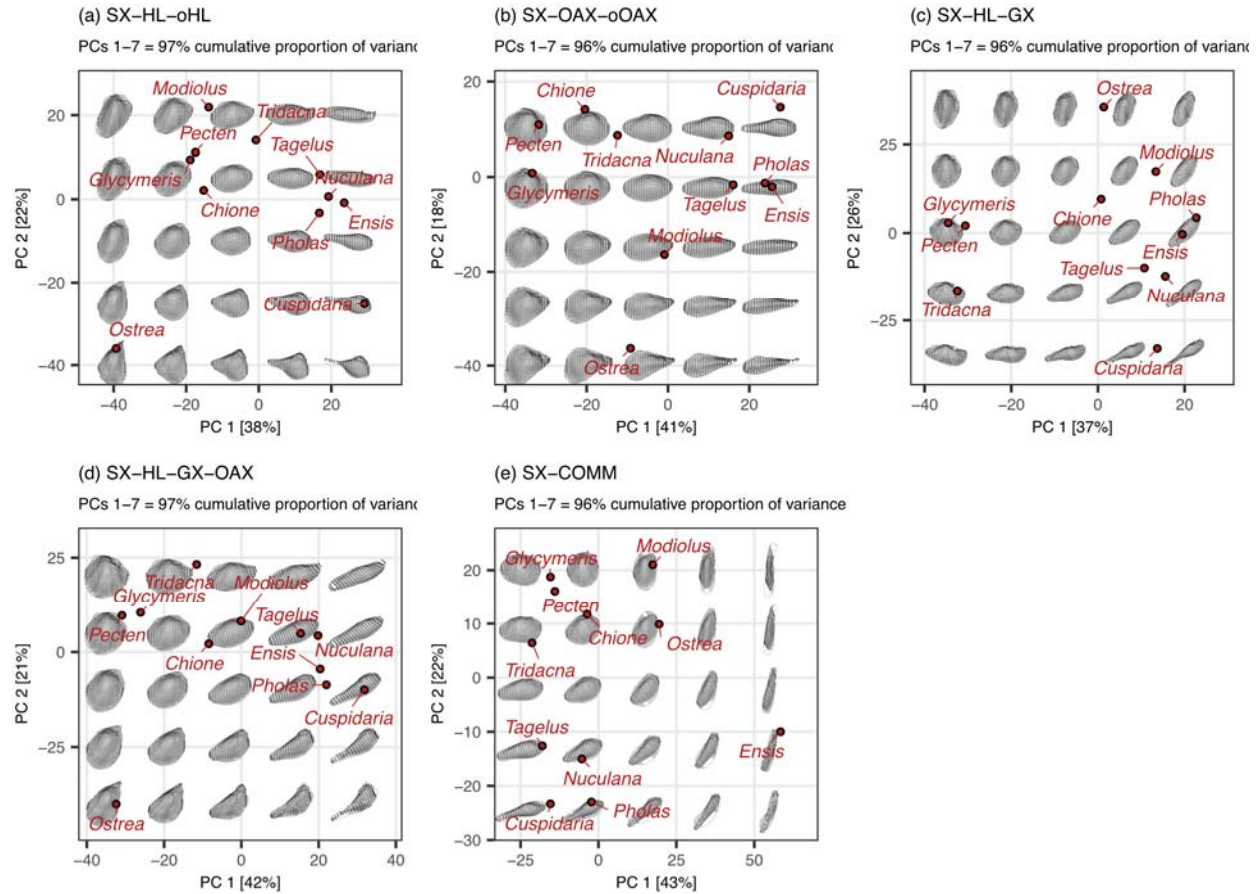**Variation in starting points of the commissure curve and orientation of the surface landmarks**

Figure S5. Placement of sliding semilandmarks along the commissure curve and the interior surface of the shell depending on orientation scheme. All landmark sets in this figure are scaled by the centroid size of the shell points and translated to the centroid of the shell commissure. Rainbow colored points indicate point order, with the most saturated red and blue as the respective initial and terminal points. (a) Commissure curve begins at the point that forms the smallest angle between the orthogonal hinge line vector and a vector originating at the centroid of the commissure curve and terminating at a point along it. Surface semilandmarks are oriented orthogonal to the hinge line. (b) Commissure curve begins at the point that forms the smallest angle between the orthogonal oro-anal axis vector and a vector originating at the centroid of the commissure curve and terminating at a point along it. Surface semilandmarks are oriented orthogonal to the oro-anal axis. (c) Commissure curve and surface landmarks oriented as in panel a. (d) Commissure curve and surface landmarks oriented as in panel a. (e) Commissure curve begins as the point nearest the beak. Surface semilandmarks are oriented orthogonal to the line connecting the 13th and 38th sliding semilandmarks on the commissure curve, which generally reflect the anterior and posterior directions.

843   **S3. Supplemental Results**
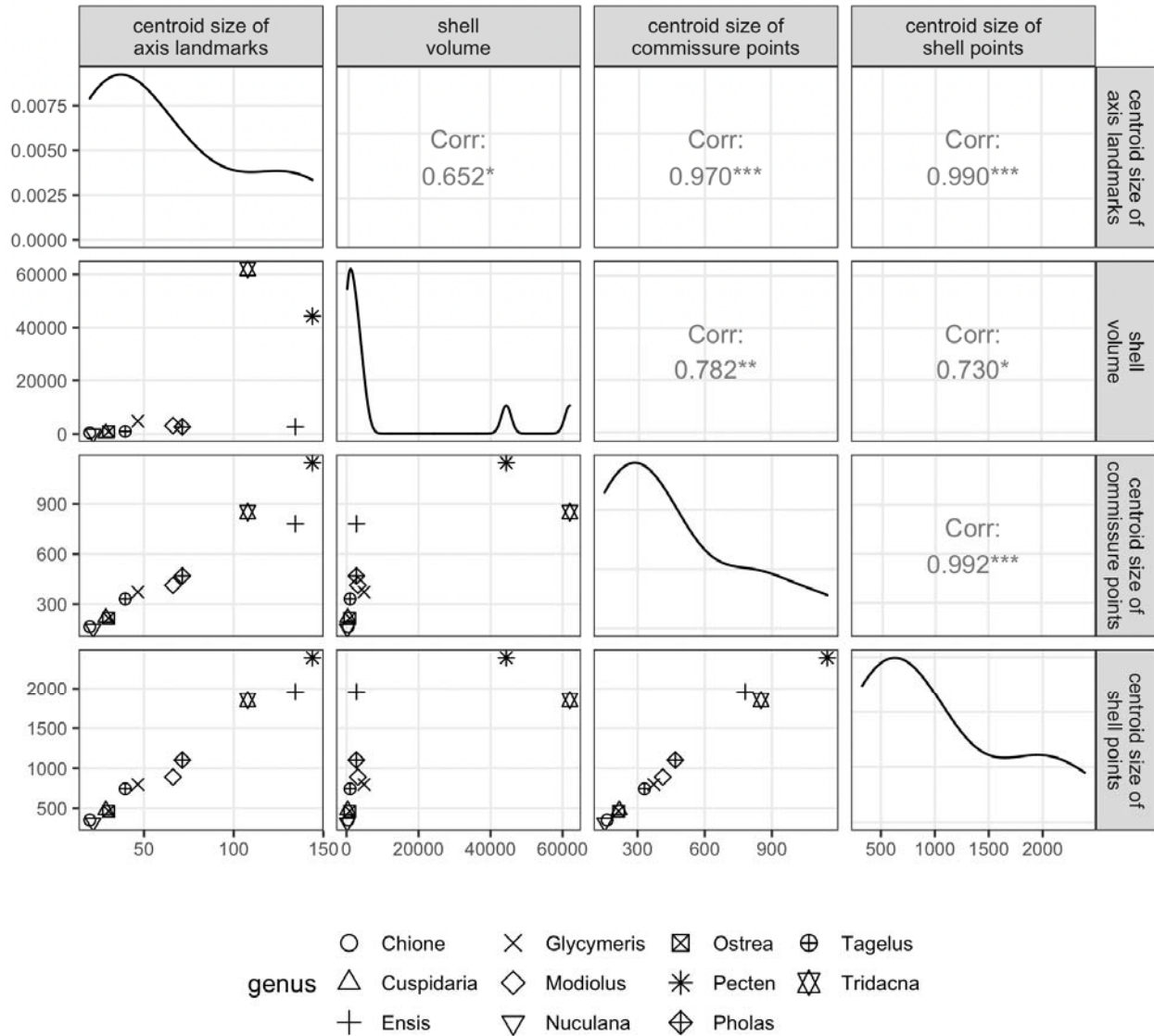
844

845   **Figure S6.** Correlations of size measures. Lower left triangle of the plot matrix shows the
846   pairwise, bivariate relationships of size measures among analyzed specimens. Diagonal of the
847   plot matrix shows density function for each size measure. Upper right triangle of the plot matrix
848   shows results of Pearson correlation tests, with asterisks denoting significance at the following *p*
849   levels: * = 0.05, ** = 0.01, and *** = 0.001.

Figure S7. Principal components analysis of the aligned sliding semilandmarks on the commissure and interior surface of the shell. All landmark sets in this figure are scaled by the centroid size of the shell points and translated to the centroid of the shell commissure. Panels a-e give the positions of specimens on the first two principal components (PCs; percentages in brackets on each axis give the proportion of total variance explained by that axis). Images of shells are projections of the shapes at their given locations in the PC1-PC2 space. Holes in the mesh surfaces are artifacts of the meshing algorithm; the black points are the true underlying data.